POLITECNICO DI MILANO

Corso di Laurea Magistrale in Ingegneria delle Telecomunicazioni
Dipartimento di Elettronica Informazione e Bioingegneria

Multicarrier-Based Optical System for Very High Capacity Transmission in Short-Range Reach

Relatore: Prof. Pierpaolo Boffi
Correlatore: Ing. Alberto Gatto

Tesi di Laurea di:
Debora Argenio, matricola 813860

Anno Accademico 2014-2015

Alla mia famiglia

"Noi vogliamo, per quel fuoco che ci arde nel cervello, tuffarci nell'abisso, Inferno o Cielo, non importa. Giù nell'Ignoto per trovarvi del nuovo."

Charles Baudelaire, *Il viaggio*

Abstract

The constant increasing demand for more and more information throughput even at the lower levels of the network in short-range reach, poses nowadays research looking for new cost-effective and scalable solutions.

While traditional copper lines and radio links approach their limits, optical systems are able to reply to such demand.

Optical fibers and directly modulated vertical cavity surface emitting lasers (VCELs) in intesity-modulated and direct-detected (IM/DD) optical systems, are the key elements to provide low-costs, flexibility and robustness to the consumer needs.

This thesis exploits frequency division multiplexing (FDM) technique to further increase the spectral efficiency of such short-range optical systems with respect to the single-carrier modulations (such as pulse amplitude modulation, PAM), while simplifying to the maximum extent the digital signal processing, which could result in prohibitive costs, unlike other multicarrier transmissions (such as orthogonal FDM, OFDM, and discrete multitone, DMT, modulation) do.

The goal of the work is to reach the highest possible capacity of the system within a minimum bit-error-rate (BER), at different single-mode fiber (able to reach distances up to few tens of kilometers) lengths.

By optimizing the number and the modulation order of the subcarriers (through "bit and power loading" algorithms), as well as different system parameters, high capacity transmission performance can be achieved.

The obtained results are notable related to those achieved in literature, and in particular considering the low-cost employed VCSEL, characterized by a narrow modulation bandwidth.

Sommario

L’ incessante domanda di un traffico dati sempre maggiore anche ai bassi livelli della rete e lungo brevi distanze, pone oggi la ricerca verso nuove, economiche e scalabili soluzioni.

Mentre i tradizionali cavi di rame e collegamenti radio mostrano i loro limiti, i sistemi ottici sono in grado di rispondere alle esigienze attuali.

Fibre ottiche e laser a cavità verticale ad emissione superficiale (VCSEL), in sistemi ottici a modulazione di intensità e rivelazione diretta (IM/DD), sono gli elementi chiave per offrire bassi costi, flessibilità e robustezza al consumatore.

Il presente lavoro di tesi sfrutta la tecnica di multiplazione a divisione di frequenza (FDM) per aumentare l’ efficienza spettrale dei sistemi ottici a corto raggio di cui sopra, rispetto alle tecniche di modulazione a singola portante (come nel caso della modulazione ad ampiezza di impulsi, PAM), e semplificando al contempo l’ elaborazione numerica del segnale, che può comportare costi proibitivi, come avviene in altre tecniche di modulazione a multi-portante (è il caso della multiplazione ortogonale a divisione di frequenza, OFDM, o della modulazione multi-tono discreta, DMT).

Lo scopo del presente lavoro è il raggiungimento della più alta capacità di trasmissione possibile del sistema, entro un minimo tasso di errore del bit (BER), ed a diverse lunghezze di fibra a singolo modo (attraverso cui è possibile raggiungere distanze dell’ ordine dei chilometri).

Ottimizzando il numero e l’ ordine di modulazione delle sottoportanti (grazie alla tecnica del "bit and power loading"), e vari parametri di sistema, è possibile raggiungere un’ elevata capacità trasmissiva.

I risultati ottenuti sono notevoli se paragonati a quelli riportati in letteratura, ed ancor più se si considera il tipo di VCSEL a basso costo utilizzato, caratterizzato da una ridotta banda di modulazione.

Acknowledgements

I would like to express my sincere thankfulness to Professor Mario Martinelli, who allowed me to develop this work at Policom laboratory, and to my supervisor Professor Pierpaolo Boffi for his precious advices, observations and suggestions.

A profound thank to my thesis mentor Eng. Alberto Gatto for his guidance, patience, encouragement and support during the work; without him this thesis would not have been possible.

I would like also to thank all the Policom members, who inspired me with their passion for the research work, and in particular Jacopo, who helped me during this thesis.

A special thank to Lorenzo for his constant support and care during the time spent together at the university, and especially in everyday life.

Thanks to the friends known during these years at university and to those who accompanied me for a longer time.

My deepest gratitude to my family and my parents for the education and principles they gave me, and for continuously supporting me.

Contents

List of Figures

Introduction

In a world continuously asking for more and more information throughput, standard solutions such as copper lines and radio links seem to approach their limits. Optical solutions propose to reply to such increasing demand not only in long and medium-range networks, but also in short-range data communication scenarios, for both professional as well as consumer applications.

The goal of this short-range data communication scenario, is to offer cost-effective and robust optical solutions at relatively short (few tens of kms) transmission distances.

The exploitation of technological solutions based on traditional single-mode fibers (SMFs), multimode glass fibers (MMFs), and low-cost vertical cavity surface emitting laser diodes (VCSELs), are therefore being proposed. These solutions feature low costs, easy handling and installation, flexibility, and robustness, which are all very suitable characteristics for consumer needs, at the expense, however, of less bandwidth when compared to long-haul transmission systems.

In order to increase the spectral efficiency of such systems, various modulation formats have been exploited: single-carrier as well as multicarrier ones.

A candidate modulation format, suitable for short-range optical communication systems, is quadrature pulse amplitude modulation (4-PAM), which shows lower complexity than subcarrier-based formats (since it is a single-carrier modulation), but, on the other hand, it shows also lower spectral efficiency [1].

In a multicarrier transmission system, such as frequency division multiplexing (FDM), or orthogonal frequency division multiplexing (OFDM), a high-speed serial data stream is divided into multiple parallel low-speed substreams which are transmitted simultaneously using different frequencies; in this way, high spectral efficiency can be achieved, and signal impairments such as dispersion can be contrasted.

Derived from the more general OFDM, discrete multitone (DMT) is a baseband

multicarrier modulation technique that is already widely employed in copper-based digital subscriber lines (DSL) systems, such as asymmetrical DSL (ADSL) and very high data rate DSL (VDSL). The main drawback of OFDM and DMT is their high peak-to-average power ratio (PAPR). Moreover, owing to the stringent requirements for high speed digital signal processing (for example > 40 GS/s to reach capacities of the order of tens Gb/s), in inverse fast Fourier transform (IFFT) and fast Fourier transform (FFT) operations, the costs may become prohibitive [2].

Owing to this criticism, the transmission technique can thus be moved to FDM in combination with multilevel modulation formats: high spectral efficiency and dispersion tolerance are still guaranteed, without the typical OFDM disadvantages [3].

As far as concerning the optical system, it can be mainly categorized as coherent and incoherent (direct-detected) systems. In general, coherent detection exhibits better sensitivity and better spectral efficiency (SE) than a direct-detected system. However, the coherent approach requires a local oscillator and extra phase and frequency offset estimation at the receiver, thus increasing the complexity of both the transmitter and the receiver. On the other hand, direct-detection requires only one photodiode at the receiver and thus it is very simple to be implemented [4].

Low-cost optical systems adopt therefore intensity-modulation and direct detection (IM/DD) technique, where only the intensity of light is modulated and not the phase.

The goal of this thesis is to study the feasibility of an optical system tailored for short-range applications, able to reach the highest possible capacity within a minimum bit error rate (BER), at different fiber lengths.

Starting from the actual state of the art and orienting the research towards the solutions which offer the best trade-offs between costs, simplicity and capacity in a consumer scenario, the strategy adopted in this thesis to design the system is based on:

- *IM/DD technique*
- *VCSEL as optical source*
- *SMF as transmission medium*
- *FDM in combination with multilevel modulation formats as transmission technique*

- *No use of any optical amplifier along the optic fiber path*

Following this approach, the number and the modulation order of the subcarriers for maximizing FDM transmission performance over an optical IM/DD channel are investigated, and different system parameters are optimized.

Chapter 1 focuses on the concept of short-range systems, pointing out its features and possible ways of realization. The chapter shows also the solutions to the problem proposed in literature, their pros and cons, and it ends with the architecture proposed in this thesis.

Chapter 2 is dedicated to the strategy adopted in this thesis.

Chapter 3 presents the characterization of the main devices employed.

Chapter 4 introduces the experimental activity, its results and performance analysis.

In the end, Conclusions sums up the starting problem, the proposed solution with its experimental results, and it suggests possible future related works.

Chapter 1

Short-range systems

1.1 Principles and realization

Nowadays, when more and more information throughput is needed, standard solutions such as copper lines and radio links show their limited scalability.

In the virtually infinite broad electromagnetic spectrum, there are only two windows that have been largely used for modern-day broadband communications. The first window spans from the long-wave radio to millimeter wave, or from 100 kHz to 300 GHz in frequency, whereas the second window lies in the infrared lightwave region, or from 30 THz to 300 THz in frequency. The first window provides the applications that we use in our daily lives, including broadcast radio and TV, wireless local area networks (LANs), and mobile phones. These applications offer the first meter or first mile access of the information networks to the end user. Nevertheless, most of the data rates are below gigabit per second (Gb/s) primarily due to the lack of the available spectrum in the RF microwave range. In contrast, due to the enormous bandwidth over several terahertz (THz) in the second window, the lightwave systems can provide a capacity of 100 Tb/s and beyond. In the late 20^{th} century, the electrical-based systems had reached a point of saturation in terms of capacity and reach. A typical coaxial transport system operated at a rate of 200 Mb/s needs to regenerate every 1 km, which is costly to operate. The natural trend was to study the lightwave communication systems, in which the data rate can be increased dramatically thanks to the realization of a laser that gives a coherent source for the transmitter, and the optical fiber as the lightwave transmission medium. Moreover, transmission distances can be substantially increased up

to thousands of kilometers by using optical amplifiers [5].

In the recent years, with the rapid increase in merging applications concerning metro and local-loop traffic, with the need for much higher communication and interconnect capacity at the lower levels of the network, short-haul communication systems over few tens of kilometers have become even more important. With respect to the long-haul systems, short-range systems require low costs and low power consumption, easy handling and installation, flexibility and scalability (at the expense, however, of less spectral efficiency, leading to lower transmission bit-rates). These requirements find their solution in optical systems based on low-cost VCSELs, with traditional SMFs, or MMFs. Such systems adopt IM/DD technique, which requires only one photodiode at the receiver, since only the intensity of light is modulated and not the phase. The most exploited modulation formats in order to increase the spectral efficiency are: 4-PAM, FDM, DMT.

1.2 Optical fiber

Optical fiber is the key element in an optical transmission system since it transports the optical signal from source to destination. The combination of low-loss and extremely large bandwidth allows high-speed signals to be transmitted over long distances before the regeneration becomes necessary. A low-loss optical fiber is manufactured from several different materials; the base row material is pure silica, which is mixed with different dopants in order to adjust the refractive index of optical fiber. The optical fiber, shown in Figure 1.1, consists of two waveguide layers: the *core* (of refractive index n_1) and the *cladding* (of refractive index n_2), protected by a coating. The majority of the power is concentrated in the

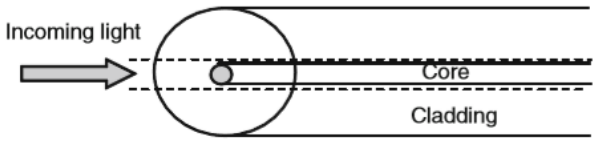

Figure 1.1: Optical fiber

core, although some portion can spread to the *cladding*. There is a difference in

refractive indices between the *core* and *cladding* ($n_1 > n_2$), which is achieved by a mix of dopants added to the fiber *core* [5].

The light coming from the optical fiber behaves like a Gaussian beam and it does not change during the propagation. As a consequence, uniqueness and continuity between the *core* and *cladding* regions must be ensured: *uniqueness* implies the same propagation wave-vector β and azimuthal index l both for the zone of the core and of the cladding; *continuity* means that the solution cannot present any discontinuity in the interface core/cladding (any discontinuity would cause the destruction of the propagating field).These conditions are respectively translated in the following *boundary equations*:

$$\beta_{core} = \beta_{cladding} = \beta \tag{1.1}$$

$$l_{core} = l_{cladding} = l \tag{1.2}$$

and:

$$R_{core}(a) = R_{cladding}(a) \tag{1.3}$$

$$R'_{core}(a) = R'_{cladding}(a) \tag{1.4}$$

where R is the radial function.

Figure 1.2 shows the *core* and *cladding* regions in the dispersion diagram. Since the optical fiber is characterized by two main zones with different refractive index, the dispersion diagram presents two straightforward lines, one related to the cladding zone ($c/n_{cladding}$), and the other related to the core zone (c/n_{core}). Fixed a certain pulsation value on the vertical axis, two wave-vectors are intercepted on the diagram: $k_{cladding}$ and k_{core} . k represents the wave-vector proper of the plane wave and β can be seen as the component of the wave-vector k in the direction of propagation of the eigen-solution (the propagation in the optical fiber); β results

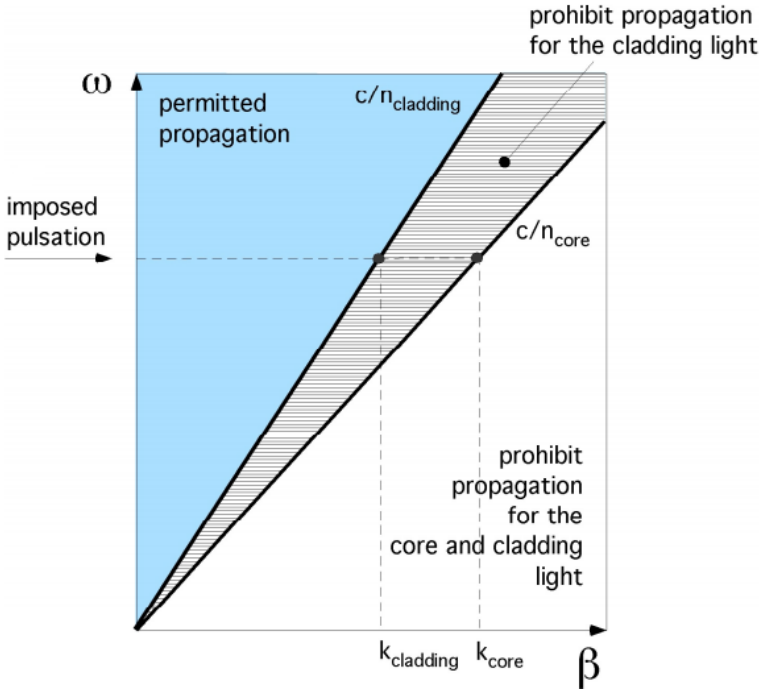

Figure 1.2: Dispersion diagram

therefore shorter than k. Since β must be unique and shorter than k, it has:

$$\beta_{cut-off} = k_{cladding}. \tag{1.5}$$

This extreme solution is called *cut-off* because it confines with the free-propagation solution: if $\beta_{cut-off}$ decreased again, it would become a generic plane wave propagation vector. It is possible to have less confined solutions, but, since the solution must be unique, this implies that, as far as concerning the cladding field, we need to penetrate in the prohibited region or, in other terms, in a region were only "evanescent" fields are allowed. Hence, for all the propagating modes of the optical fiber (except for the cut-off point), the following relationship holds:

$$k_{cladding} < \beta < k_{core}. \tag{1.6}$$

As shown in Figure 1.3, at each pulsation value it will correspond one value of β. As far as the pulsation is growing, β approaches the c/n_{core} and, for sufficient

high pulsations, more than one β is possible: we begin the multimode propagation. The figure shows also the Pythagorean representation of β and k [6].

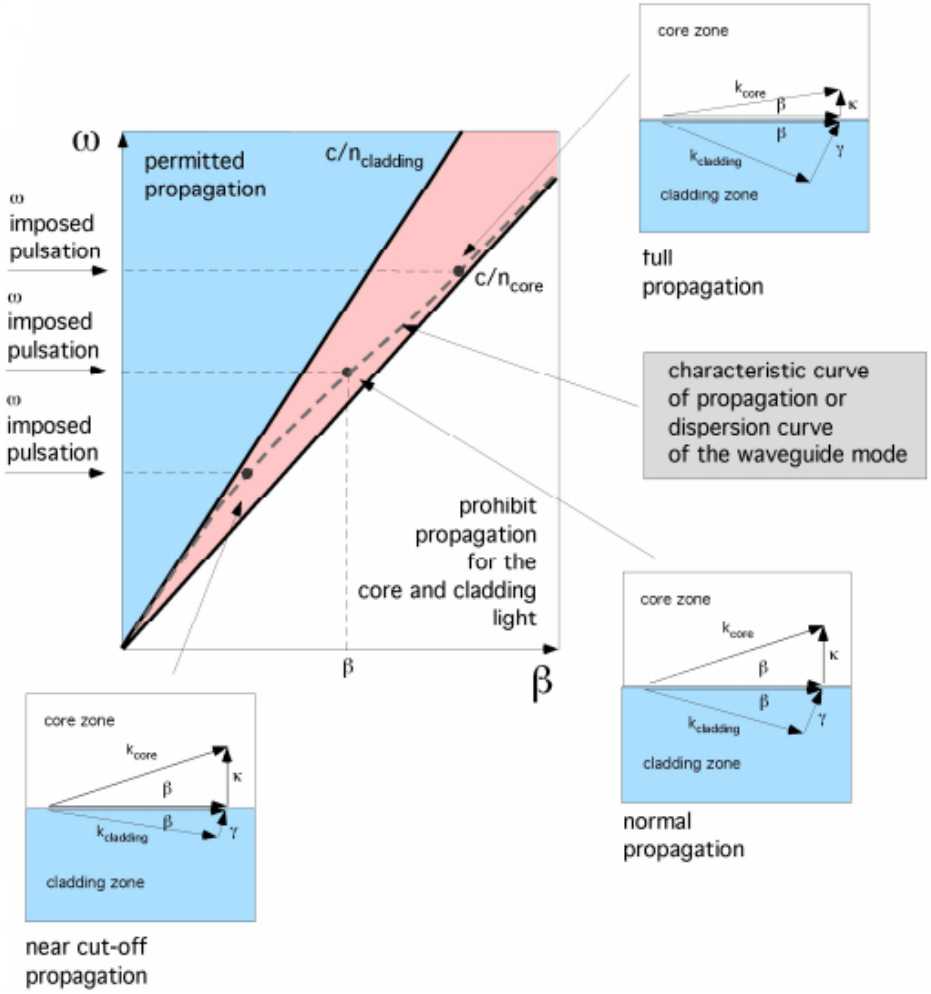

Figure 1.3: Multimodal dispersion diagram

Two types of optical fibers can be therefore distinguished: single-mode fibers, and multimode fibers.

1.2.1 Single-mode fiber

Single-mode fibers (SMFs) are designed so that they support only a single propagation mode, called *fundamental mode*, per polarization direction for a given wavelength. Modes are the possible auto-solutions of the Bessel equations for

the waves in a cylindrical space (which are obtained by combining Maxwell's equations and the boundary conditions). The fundamental mode occupies the central part of the optical fiber and it has an energy maximum at the axis of the optical fiber core. Its radial distribution can be approximated by a Gaussian curve.

SMFs introduce the *chromatic dispersion*, defined as "the variation of the *specific propagation delay* τ_g in function of the frequency", and it has two components: *waveguide dispersion* and *material dispersion*. Given a length l of optical fiber, the propagation delay is:

$$t = \frac{l}{v_g} \tag{1.7}$$

where v_g is the group velocity:

$$v_g = \frac{d\omega}{d\beta}. \tag{1.8}$$

The *specific propagation delay* τ_g is the delay for unit of length:

$$\tau_g = \frac{1}{v_g} = \frac{d\beta}{d\omega}. \tag{1.9}$$

By definition, the *chromatic dispersion* β_2 is:

$$\beta_2 = \frac{d\tau_g}{d\omega} = \frac{d}{d\omega}\left(\frac{d\beta}{d\omega}\right) = \frac{d^2\beta}{d\omega^2} \tag{1.10}$$

As shown in Figure 1.4, the propagation curve in fiber moves from the core to the cladding asymptote. As a result, it presents an unavoidable inflection which causes a change in the derivative sign $\frac{d\omega}{d\beta}$, so originating the first component of the chromatic dispersion: the *waveguide dispersion*.

The other component of the chromatic dispersion is the *material dispersion*, and it is due to the fact that the segments which constitute the asymptotes in the dispersion diagrams are not straight lines, but they are curves which evolve in function of the frequency [6].

As it will be discussed in section 1.8, SMFs are usually used in combination

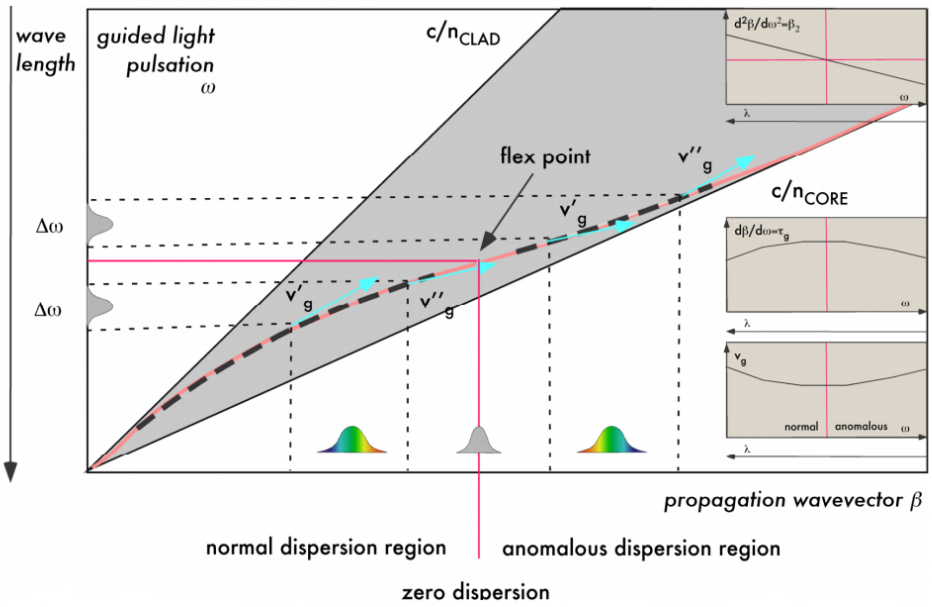

Figure 1.4: Chromatic dispersion

with 1550-nm VCSELs for relatively short-range communications (few tens of kilometers) [7–10]

1.2.2 Multimode fiber

In addition to the impairments introduced by SMFs (*i.e.* chromatic dispersion), multimode fibers (MMFs) are characterized also by the *multimode dispersion*, which affects the propagation sooner than the chromatic dispersion. MMFs transfer the light through a collection of spatial transversal modes. Each mode occupies a different cross section of the optical fiber *core* and it takes a distinguished path along the optical fiber. The difference in mode path lengths in MMFs produces a difference in the arrival times at the receiving point, originating the *multimode dispersion*, or *intermodal dispersion*, which causes the signal distortion, leading to limitations in the signal bandwidth. SMFs effectively eliminate *multimode dispersion* by limiting the number of propagating modes to a fundamental one. The number of modes M that can effectively propagate through an optical fiber is determined by the *normalized frequency* (V parameter or V number):

$$M \approx \frac{V^2}{2}. \tag{1.11}$$

The *normalized frequency V* is defined by:

$$V = \frac{2\pi a}{\lambda}\sqrt{n_1^2 - n_2^2} \tag{1.12}$$

where *a* is the fiber core radius, λ is the carrier wavelength, and n_1 and n_2 are the refractive indices related to the fiber core and the fiber cladding, respectively. Each mode propagating through the fiber is characterized by its own propagation constant β; introducing the *normalized propagation constant b*:

$$b = \frac{\beta^2 - (2\pi n_2/\lambda)^2}{(2\pi n_1/\lambda)^2 - (2\pi n_2/\lambda)^2} \tag{1.13}$$

which is related to the *normalized frequency V* by:

$$b(V) \approx (1.1428 - 0.9960/V)^2, 1.5 \leq V \leq 2.5, \tag{1.14}$$

the *multimode dispersion* can be effectively eliminated by limiting the number of propagating modes to a fundamental one:

$$V \leq V_c = 2.405 \tag{1.15}$$

with V_c being the cutoff frequency. The cutoff frequency is controlled by keeping the core radius small and the normalized index difference $\Delta = (n_1 - n_2)/n_1$ between 0.2% and 0.3% [5].

The *multimode dispersion* limits the use of MMFs to few hundreds of meters: they are widely employed in local area networks, such as enterprise in-building and datacenter backbones, but also short-distance server/computer interconnects.

As it will be discussed in section 1.8, MMFs are often used in combination with 850-nm VCSELs for short-range communications (few hundreds meters) [11–15].

1.3 Intensity-modulation and direct-detection (IM/DD)

Due to costs reasons, short-range optical communication systems mainly employ intensity-modulation and direct-detection (IM/DD). These systems do not need such high levels of performance like long-haul coherent systems because of the much shorter reach. Moreover, due to its enormous market volume and low sharing factor, it is essential that the cost level of short-range optical communication systems is lowered to the minimum. It is therefore most straightforward and easy to modulate the intensity of an optical source such as an LED or a laser diode just by modulating its driving current. Consequently, at the receiver side, only the intensity of the received optical signal needs to be detected. A simple photodiode is enough to detect this intensity, making an IM/DD optical communication system the cheapest system for transmitting information by optical means. However, such a cost advantage also comes at the expense of lower performance as a result of lower spectral efficiency, leading to lower transmission bit-rates than achievable by coherent systems [2]. In fact, IM/DD systems adopt primarily on-off keying (OOK) as modulation format. Only in the recent years, further modulation formats, such as FDM or OFDM, have been exploited in order to increase the spectral efficiency of such systems (see paragraph 1.4).

Figure 1.5 shows a block diagram of an IM/DD channel model.

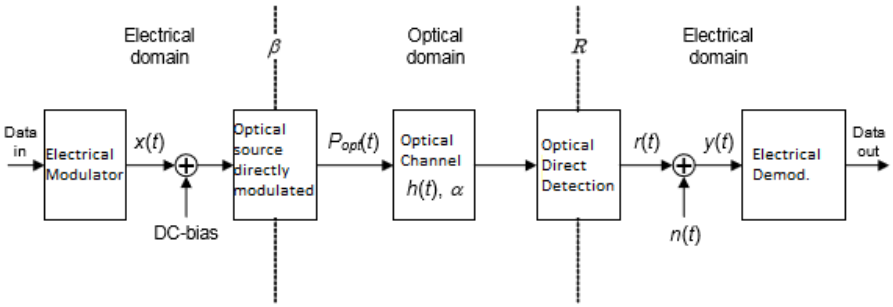

Figure 1.5: The optical IM/DD channel model

First, an electrical modulator is used to modulate the incoming data into the appropriate modulation format. This results in a transmitted electrical current $x(t)$, which is used to drive an optical intensity-modulated source such as an LED or a laser diode. $x(t)$ is considered to be an alternating current (AC) coupled, bipolar

signal, so that its mean value $\langle x(t) \rangle = 0$. Due to the fact that only the intensity of light is modulated and detected in an IM/DD channel, a unipolar modulated signal is needed to drive the optical intensity of the light source. This is achieved by adding a DC bias to $x(t)$.

Figure 1.6 shows a model of an ideal linear optical intensity modulation.

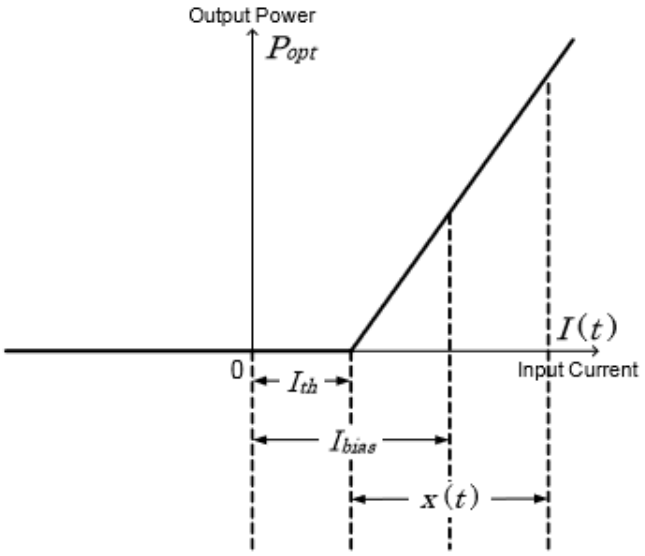

Figure 1.6: Ideal intensity modulation model

Using this model, it is assumed that no optical power is emitted when the driving current is below the threshold value of I_{th}, and the optical power emission is linearly proportional to the driving current when this current is above I_{th}. Moreover, there is no saturation effect for infinite values of the driving current.

In the real cases, however, saturation effect is present and the laser current must be chosen in the linear region between an upper threshold value and the saturation value.

After transmission over the channel, the optical signal is detected by a receiver which is assumed to consist of a photodiode and a trans-impedance amplifier. The received electrical signal from the photodetector $y(t)$ in V, which is assumed to be passed through a DC-block, can be written as:

$$y(t) = r(t) + n(t) \tag{1.16}$$

where $r(t)$ is the noiseless received electrical signal from the photodetector and $n(t)$ is additive noise, which in an ideal system is white Gaussian noise (AWGN), and represents only the thermal noise resulting from the trans-impedance amplifier in the receiver. Because $y(t)$ is assumed to be passed through a DC-block, the noiseless received electrical signal $r(t)$ is AC-coupled (*i.e.* its DC component is removed), resulting in:

$$r(t) = RG\alpha[P_{opt}(t) - P_{mean}] \otimes h(t) = RG\alpha\beta x(t) \otimes h(t) \tag{1.17}$$

where R is the responsivity of the photodiode in A/W$_o$, G is the trans-impedance gain of the photodetector in V/A, α is the channel attenuation and $\otimes$ denotes the linear convolution between the modulated part of the transmitted optical power $\beta x(t)$ and $h(t)$. $h(t)$ represents the normalized, optical intensity fiber channel impulse response [2].

1.4 Modulation formats

There are two main possibilities for increasing the spectral efficiency in IM/DD links for short-range applications: *single-carrier modulation* and *multicarrier transmission*.

In the *single-carrier modulation* data are carried on a single main carrier. This is the "conventional" modulation format that has been the workhorse in optical communications for more than three decades: starting from the binary on-off keying (OOK) format, many variants have been widely developed, up to quaternary pulse amplitude modulation (4-PAM).

In the second category of modulation techniques, *multicarrier transmission*, data are carried through many closely spaced subcarriers. Frequency division multiplexing (FDM) and orthogonal frequency division multiplexing (OFDM) are the typical examples [5].

In the following, the most exploited modulation formats concerning the short-reach networks applications and the IM/DD systems will be discussed.

1.4.1 Single-carrier modulation

On-off keying

On-off keying (OOK) is the simplest form of digital modulation: a series of logical "1" and "0" is simply obtained by switching on and off the carrier.

Figure 1.7 shows an example of OOK modulation, where "0" is represented by having the carrier "off" (*i.e.* its amplitude equals to 0), and "1" is represented by having the carrier "on" (*i.e.* choosing a certain amplitude A).

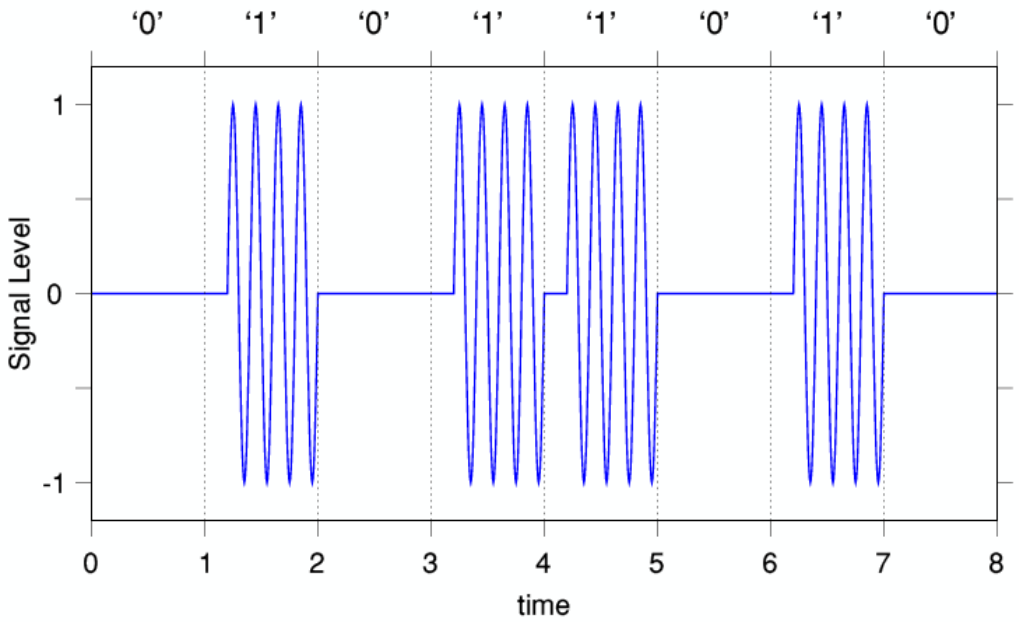

Figure 1.7: On-off binary keying

The transmitted signal is divided into a series of timed chunks, which can assume value "0" or "1"; in the example, a series of bits "01011010" is transmitted.

OOK modulation signal can be written as:

$$S(t) = a\sin(2\pi ft + \phi) \tag{1.18}$$

where $a = 0$, $\phi = 0$ when bit "0" is transmitted, and $a = A$, $\phi = 0$ when bit "1" is transmitted.

Pulse amplitude modulation

Pulse amplitude modulation (PAM) is the transmission of data by varying the amplitude (power level) of the individual pulses in a regularly timed sequence of electrical or electromagnetic pulses. The number of possible pulse amplitudes is usually some power of two so that the resulting output signal can be digital.

Figure 1.8 shows a transmission and reception pulse amplitude modulation scheme.

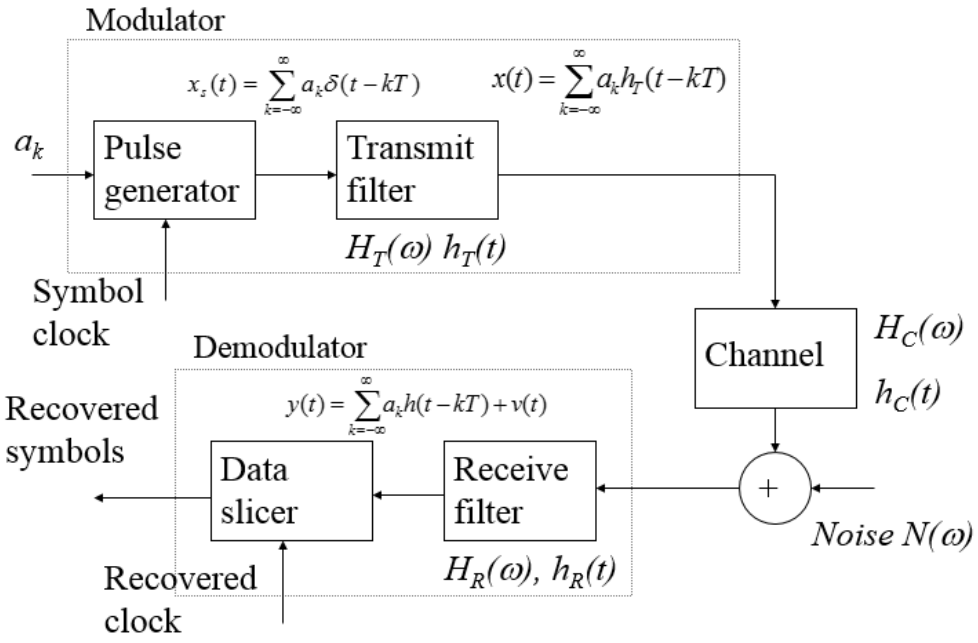

Figure 1.8: PAM scheme

In binary PAM, each symbol a_k takes only two values, A_1 and A_2; in a multi-level M-ary system, symbols may take M values, A_1, A_2 ,... A_M.The modulator converts discrete amplitude serial symbols (bits in a binary system) a_k to analogue output pulses which are sent over the channel. The demodulator reverses this process.

The PAM output signal is generated from a train of weighted impulse functions:

$$x_s(t) = \sum_{k=-\infty}^{\infty} a_k \delta(t - kT) \tag{1.19}$$

where T is the signaling period, which passes through a transmit filter $h_T(t)$, so that it has:

$$x(t) = \sum_{k=-\infty}^{\infty} h_T \delta(t - kT). \tag{1.20}$$

The transmitted signal $x(t)$ passes then through the channel $H_C(w)$ and the receiver filter $H_R(w)$. The overall frequency response is therefore:

$$H(w) = H_T(w) H_C(w) H_R(w). \tag{1.21}$$

Hence, the signal at the receiver filter output is:

$$y(t) = \sum_{k=-\infty}^{\infty} a_k h(t - kT) + v(t) \tag{1.22}$$

where $h(t)$ is the inverse Fourier transform of $H(w)$ and $v(t)$ is the noise signal at the receiver filter output. The data slicer performs then the data detection.

Figure 1.9 shows an example of modulated PAM signal representation [16].

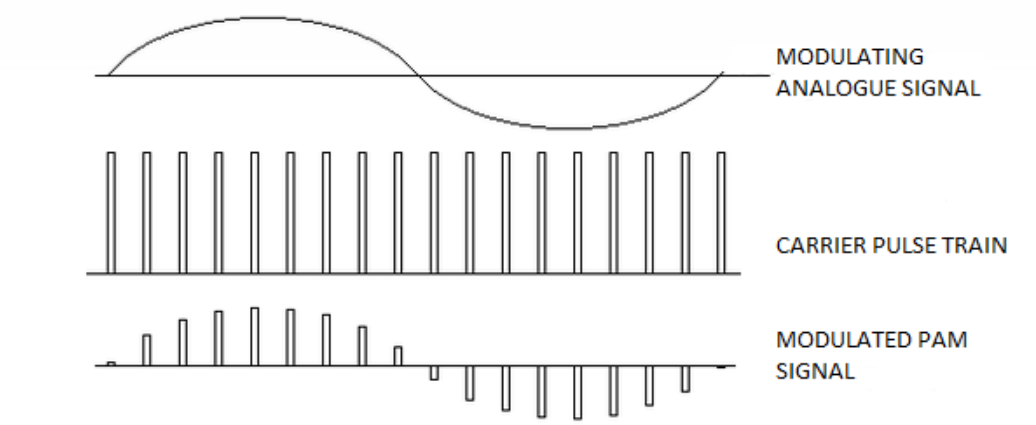

Figure 1.9: example of modulated PAM signal representation

The main advantages of the multiple subcarrier approaches are easier electronic equalization and increased robustness to effects of modal dispersion due to reduced

symbol rates. A general disadvantage of IM/DD subcarrier schemes, compared to PAM, is worse sensitivity, in terms of optical received power. Another disadvantage of the subcarrier schemes is their implementation complexity. PAM offers probably the lowest implementation complexity of all multilevel modulation formats with spectral efficiency of 2 bits/second/Hz.

If higher spectral efficiency is needed, 4-PAM (4 intensity levels, symbols, with 2 bits per symbol) [17], with forward error correction (FEC) would be a good choice from the sensitivity point of view, since it can double the data rates, with only small increase in required received optical power [18]. 4-PAM is therefore a typical modulation format employed in the short-reach networks [9–13]. The 4-PAM bit-rate requires higher speed photoreceivers in order to be further increased [12].

1.4.2 Multicarrier transmission

Frequency division multiplexing

In frequency division multiplexing (FDM), a frequency band is divided into a series of non-overlapping frequency sub-bands in order to transmit various signals simultaneously on the same medium. The frequency spectrum is divided into several logical channels, giving each user exclusive possession of a particular frequency band. For each channel, a carrier frequency is assigned. Transmitting signal is associated to a particular channel and it is modulated on the correspondent carrier frequency. In order to avoid overlaps, channels must be separated by strips of unused bandwidth: *guard bands*. The various channels are then combined by a linear summing circuit in the multiplexer, and the resulting signal is transmitted along the single channel. The carriers used to modulate the individual message signals are called *sub-carriers*, shown as f_1, f_2, ..., f_n in Figure 1.10. At the receiver side, the signal is applied to a bank of band-pass filters, which separates the individual frequency channels. The band pass filter outputs are then demodulated and distributed to the different output channels as shown in Figure 1.11.

In Figure 1.12, the FDM use is represented.

In principle there is flexibility for each sub-band to employ a different modulation scheme. With quadrature amplitude modulation (QAM), two independent baseband signals are modulated onto a sine and a cosine carrier with the same frequency $\omega\nu$ which gives an unsymmetric spectrum. As a result, the spectral efficiency is doubled [19]. Another widely adopted modulation on the subcarriers

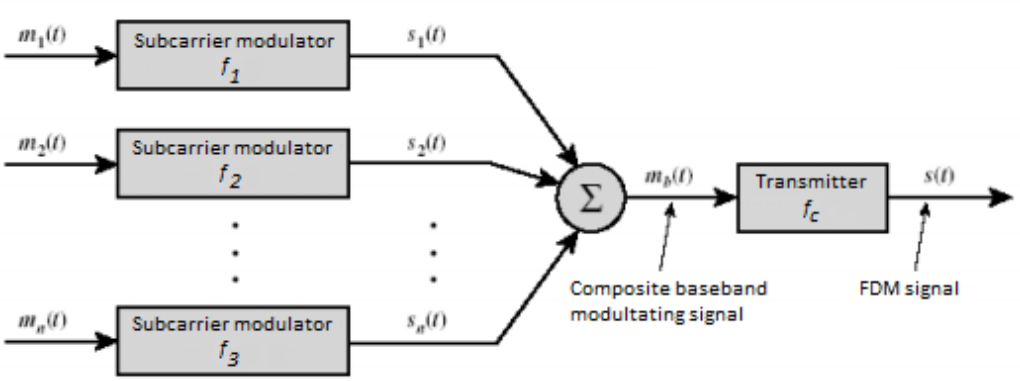

Figure 1.10: FDM transmitter block diagram

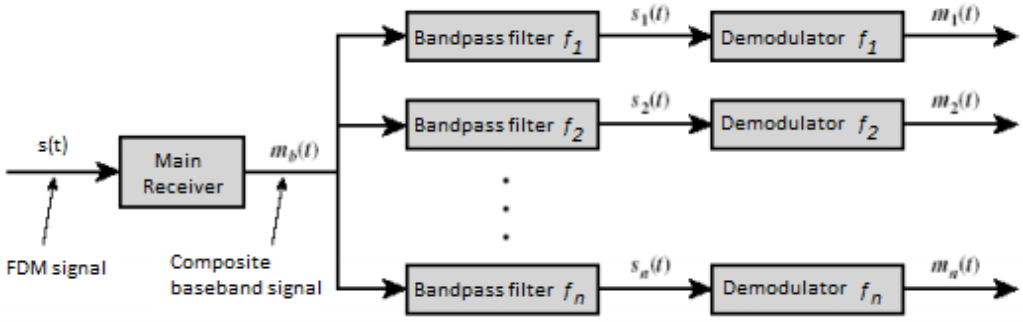

Figure 1.11: FDM receiver block diagram

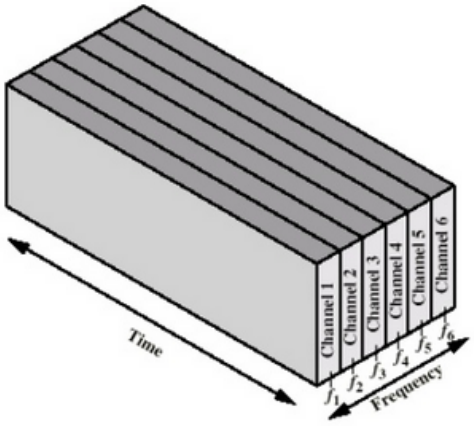

Figure 1.12: FDM use

is phase-shift keying (PSK), where no more the amplitude but the phase of a signal is modulated. However, with more than 8-order PSK, the error rate becomes too high, and it is better to employ a different modulation scheme, such as QAM.

Orthogonal frequency division multiplexing

Orthogonal frequency division multiplexing (OFDM) is a special case of FDM, in which the various *sub-carriers* are orthogonal. The orthogonality condition is verified if:

$$\Delta f = \frac{1}{T_s} \tag{1.23}$$

where $T_s = \frac{N}{R}$ is the duration of the symbols transmitted on the sub-carriers, with N the number of signals to be transmitted in parallel, and R the rate in bit/s.

The resulting signal transmitted along the single channel is:

$$s(t) = \sum_n a_n \exp(j2\pi f_n t) \tag{1.24}$$

with $0 \leq t \leq T_s$, $f_n = \frac{n}{T_s}$, $0 \leq n \leq N-1$. The N sub-carriers at frequency f_n are therefore modulated in amplitude (tipically with QAM), with the symbols $a_o, a_1, ..., a_{N-1}$. Since the sub-carriers are orthogonal, such symbols do not suffer from mutual-interference. In Figure 1.13, an example of the frequency representation of an OFDM signal with four carriers is shown.

Figure 1.14, shows the OFDM modulator and demodulator principles. From the N symbols to be transmitted $a_o, a_1, ..., a_{N-1}$, the N complex values $s_o, s_1, ..., s_{N-1}$ are generated through inverse fast Fourier transform (IFFT). Then, after the parallel/serial conversion, the real ($x(t)$) and imaginary part ($y(t)$) of the samples are generated through digital-to-analogue conversion. Such analogue signals $x(t)$ and $y(t)$ are then transmitted along the channel after amplitude modulation on the carrier f_0. On the receiver side, the carrier f_0 is demodulated and the signals $x(t)$ and $y(t)$ are extracted. The complex values s_k can be then determined; after fast Fourier transform (FFT), the symbols a_n are reconstructed by means of a data detector (because of the noise presence) [20].

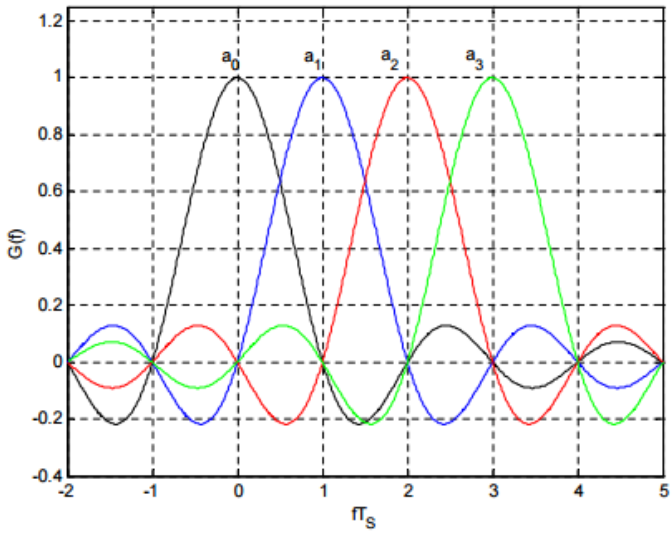

Figure 1.13: example of an OFDM signal with four carriers

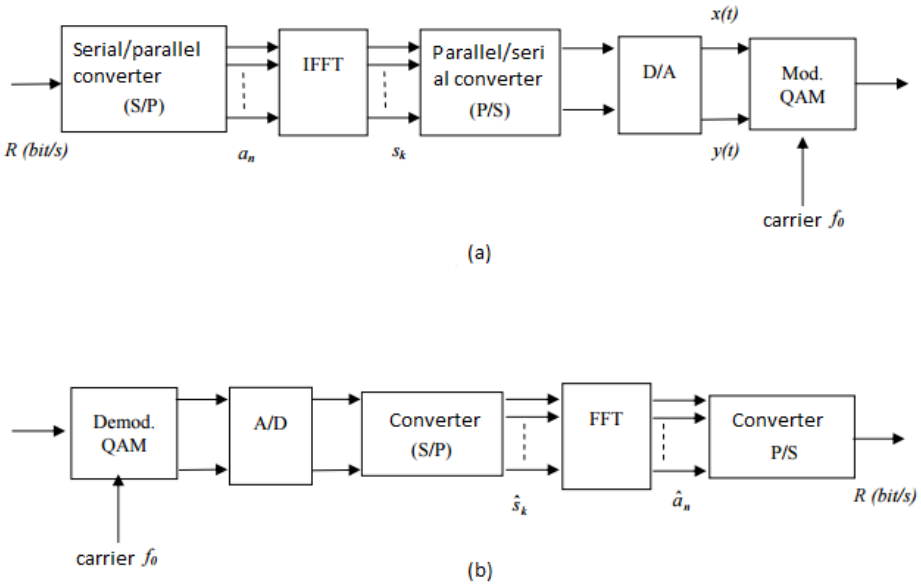

Figure 1.14: OFDM modulator (a) and demodulator (b)

Discrete multitone modulation Discrete multitone (DMT) modulation is a baseband version of OFDM. Contrary to OFDM, the DMT modulator output signal after the IFFT is real-valued and no inphase and quadrature-phase (IQ-) modulation onto a radio frequency (RF) carrier is required. As a result, only a single digital-to-analog converter (DAC) and a single analog-to-digital converter (ADC) is needed to respectively generate and capture a DMT sequence. DMT is widely employed in IM/DD systems exactly because it is a real modulation.

In Figure 1.15, the principle of DMT is shown. In order to achieve a real-valued,

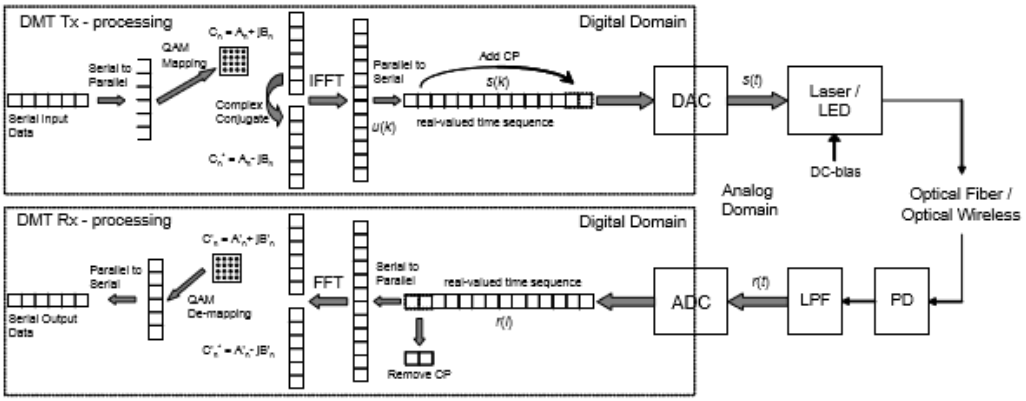

Figure 1.15: Block diagram of DMT over an optical IM/DD channel. DAC: digital-to-analog converter, ADC: analog-to-digital converter, LED: light-emitting diode, PD: photodetector, LPF: low-pass anti-aliasing filter, CP: cyclic prefix.

baseband DMT transmission sequence consisting of N subcarriers, a $2N$-point IFFT is needed. For the $2N$ inputs of the IFFT, indexed by $n = 0, 1, ..., 2N-1$, the first half are assigned the values C_n and the second half have to be assigned the complex conjugate values of C_n, following the Hermitian symmetry property given by:

$$C_{2N-n} = C_n^{\star}. \tag{1.25}$$

Following this, the output $u(k)$ of the $2N$-point IFFT is always real-valued. A cyclic prefix (CP) is added to $u(k)$ before D/A conversion. The CP is a copy of

the last fraction of $u(k)$, which is inserted in front of $u(k)$. When no CP is used, demodulation with the FFT will result in inter-carrier interference. On the other hand, the inclusion of a CP comes at the expense of additional redundancy [2].

1.5 Dispersion tolerance in multicarrier transmission

Systems for short range applications are severely affected by fiber dispersion when operating at high bit rates. Additional issues are related to the total electrical signal bandwidth occupancy (B_s), which is required to achieve high data rate. Specifically, the limited bandwidth of some electrical components such as DACs and ADCs can degrade the overall system performance.

In OFDM and DMT, the use of a CP confers robustness to the transmission, but it also requires additional bandwidth occupancy.

A possible solution to enhance resilience towards system impairments and increase system capacity for high volume of traffic is *bit loading* (BL) and *power loading* (PL). BL and PL introduce flexibility in the system and robustness against transmission impairments by allocating different number of bits and power to the subcarriers according to the channel profile. Different loading algorithms have been proposed in the literature to overcome *chromatic dispersion* (see section 1.2) and enhance the system performance. These algorithms can be implemented considering different criteria: (i) BER minimization for fixed data rate and transmit power constraints, (ii) rate maximization for a fixed energy constraint, and (iii) energy minimization at a given data rate. Cases(ii) and (iii) are usually referred to as *rate-adaptive* (RA) and *margin-adaptive* (MA) problems, respectively [21]. A well-known algorithm that solves the RA and MA problems is the *water-filling*. This algorithm starts by discarding the subcarriers that are least energy-efficient from information transmission, and redistributing the energy to more efficient subcarriers to support higher data rates. The non-integer number of allocated bits per subcarrier are then rounded to the nearest integer and the corresponding energy is in- or decreased to support the newly-allocated number of bits at the same performance [22].

Bit and power loading will be further investigated in Chapter 2, section 2.2.

1.6 IM/DD system in multicarrier transmission

In case of direct modulation of the optical source employed in the system, we can exploit a purely real signal to modulate the intensity of the light emitted by the source.

Remembering that:

$$f(t)\cos(\omega_c t) \leftrightarrow \frac{1}{2}F(\omega+\omega_C)+\frac{1}{2}F(\omega-\omega_C) \tag{1.26}$$

for any real-valued signal there exists "conjugate symmetry" in the Fourier transform, *i.e.*:

$$F(-\omega) = F^*(\omega). \tag{1.27}$$

Thus, it is possible to employ even high-order level modulations on the sub-bands of a multicarrier transmission, and directly detect them. Since conjugate symmetry occurs, all information is contained in either the positive or the negative frequency components, and, as a consequence, the direct detection will result in the modulus squared of the input signal, at the expense however of a transmitted information reduction of half the bandwidth.

1.6.1 Optical double-side band

The received directly detected signal in case of multicarrier transmission consists of a number of mixing products. After intensity modulation, the modulated optical signal results double-side banded (ODSB), see also Chapter 3, section 3.3.2. As explained in section 1.6.2, an optical filter can be used after intensity modulation in order to suppress one sideband, thus obtaining an optical single sideband signal (OSSB). Although SSB is immune to subcarriers-to-subcarriers mixing interference (SSMI) and frequency fading (FF), (see Chapter 3, section 3.3.2), the structure of the system required is more complicated and higher demand on costly components compared to that of DSB transmission.

As explained in [23], the received directly detected signal in case of DSB modulation of an input multicarrier transmission (FDM), is characterized by a series of mixing products. Figure 1.16 shows the effects of such mixing terms on

the optical and electrical spectra:

- optical carrier × FDM subcarriers
- FDM subcarriers × FDM subcarriers
- optical carrier × noise (called "noise 1" in Figure 1.16)
- FDM subcarriers × noise (called "noise 2" in Figure 1.16).

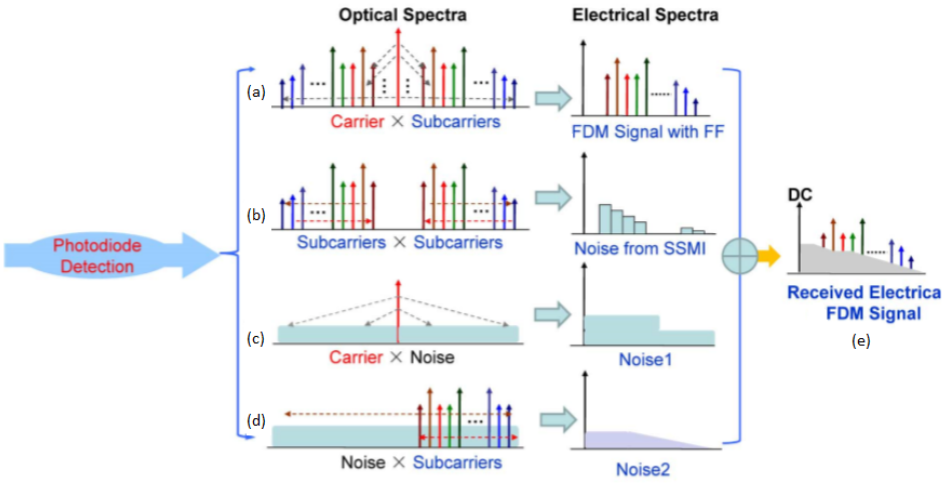

Figure 1.16: Received signal: (a) optical carrier × FDM subcarriers; (b) FDM subcarriers × FDM subcarriers; (c) optical carrier × noise; (d) FDM subcarriers × noise; (e) degraded signal.

Due to FF, the high-frequency subcarriers of the received FDM are degraded. The beating between FDM subcarriers such as (b) shown in Figure 1.16 will generate SSMI. Because SSMI of the subcarriers which are close to the optical carrier is severe, the received FDM subcarriers close to the optical carrier will be suffered from interference severely. This will degrade the received FDM signal. In (c) and (d), there will produce some in-band electrical noise, which degrade the SNR and the receiving sensitivity. After the low-pass filter, the degraded signal as shown in (e) is obtained.

1.6.2 Optical single-side band

Single-side band (SSB) modulation is basically a derivative of amplitude modulation (AM). By removing some of the components of the ordinary AM signal, it is possible to significantly improve its efficiency. SSB uses only one side band to provide the final signal: only the upper side band (the portion above the carrier frequency), or the lower side band (the portion below the carrier frequency), is transmitted, as shown in Figure 1.17 [24]. In practice, different formats of SSB

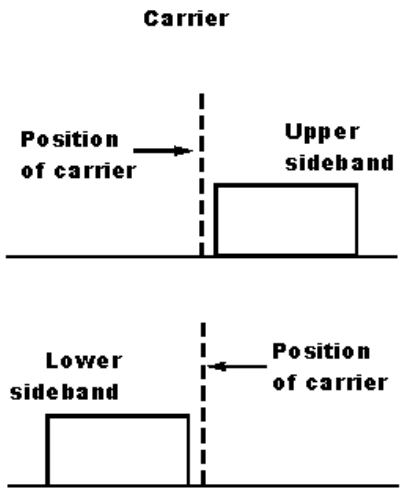

Figure 1.17: Single-side band modulation showing upper and lower side band signals

modulation can be used: the second side band can be only partly cut off, or it can carry a different modulation, and the carrier can be fully transmitted, reduced, or suppressed (this is the most widely used and efficient case). SSB modulation provides a considerably more efficient form of communication when compared to ordinary AM, in terms of the radio spectrum used, and also the power used to transmit the signal:

- If the carrier is not transmitted, this enables a 50% reduction in transmitter power level for the same level of information carrying signal (for an AM transmission using 100% modulation, half of the power is used in the carrier and a total of half the power in the two side bands, so that each side band has a quarter of the power).

- If only one side band is transmitted, there is a further reduction in transmitter power.
- If only one side band is transmitted, the receiver bandwidth can be reduced by half. This improves the signal-to-noise ratio (SNR) by a factor of two, *i.e.* 3 dB, since the narrower bandwidth used will be affected by less noise and interference [25].

Such increase in performance comes however at the expense of some additional complexity: with a suppressed carrier, the receiver requires an internal oscillator to be able to reconstruct the signal. While an oscillator can be made cheaply, providing an oscillator that can cover the range of all possible frequencies in your band and be stable does not come cheaply. Therefore, such SSB systems are usually limited to expensive applications (television signals), or situations where the improved performance is essential (like the military).

In [26], an example of OSSB transmission is shown. The direct detection technique is implemented in three different ways. These have various degrees of optical complexity at the transmitter, but they all use a single direct-detection photodiode at the receiver side, no laser is required at the receiver. An OFDM signal is investigated, but the analysis can be extended to a generic multicarrier modulation with baseband input signals. An OSSB input signal and a component at the optical carrier frequency are transmitted. A frequency guard band separates the input signal from the optical carrier.

Figure 1.18 shows the transmitter side of such DD-system. Figure 1.18(a) shows the details of the first transmitter design. A single input optical modulator is used to generate an ODSB signal and then one side band is suppressed using an optical filter. The electrical input to the optical modulator is a real, baseband signal and only one DAC is required. The details of the second design are shown in Figure 1.18(b). The single DAC of the first design is replaced by two DACs and an electrical RF upconversion stage. This allows the complex baseband input signal to be mixed with an RF carrier before driving the single input optical modulator. The width of the guard band is determined by the RF frequency, and so all subcarriers except the dc subcarrier can be used to carry data. The analog upconversion allows flexible placement of the signal spectrum relative to the optical carrier, and the RF frequency is independent on the DAC sample rate. As in the first design, an optical filter is used to suppress one side band. For a given data rate, this design requires a DAC sample rate of approximately one quarter that of the first

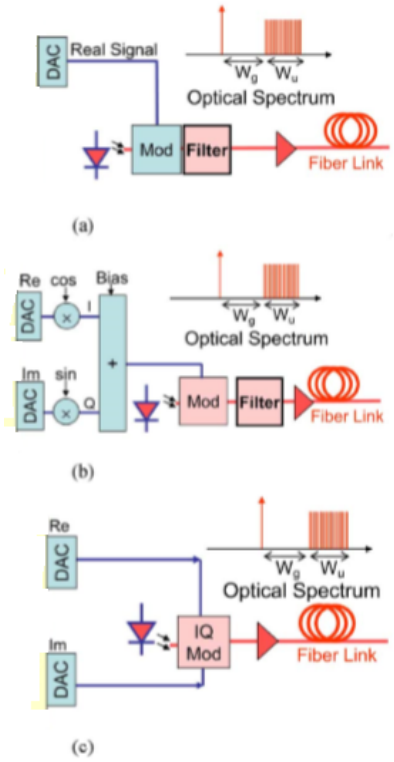

Figure 1.18: DD-OSSB transmitters: (a) using a real signal and an optical filter; (b) using upconversion and an optical filter; (c) without optical filter.

design. But the addition of analog mixers with such high frequency and bandwidth requirements may cause problems with frequency synchronization and inphase (I) and quadrature (Q) balance. The third transmitter design, which is shown in Figure 1.18(c), generates an OSSB analytic signal and its real and imaginary components are used for the I and Q inputs of the complex optical modulator for OSSB transmission without an optical filter. The frequency guard band is created by setting the corresponding inputs to zero. This design requires two DACs, each with the same sample rate as the first design.

1.7 Vertical-cavity surface-emitting laser (VCSEL)

Vertical-cavity surface-emitting lasers (VCSELs), are semiconductor lasers, more specifically laser diodes with a monolithic laser resonator, where the emission of the light is perpendicular to the chip surface. The resonator (cavity) is realized with two semiconductor Bragg mirrors. Between those, there is an active region (gain structure) with typically several quantum wells and a total thickness of only a few micrometers. In most cases, the active region is electrically pumped with a few tens of milliwatts and generates an output power in the range from 0.5–5 mW, or higher powers for multimode devices. The current is often applied through a ring electrode, through which the output beam can be extracted, and the current is confined to the region of the resonator mode using electrically conductive (doped) mirror layers with isolating material around them. VCSELs can have a good beam quality only for fairly small mode areas (diameters of a few microns) and are thus limited in terms of output power.

The VCSEL has several advantages over edge-emitting diodes: it is cheaper, easier to test, and more efficient. In addition, the VCSEL requires less electrical current to produce a given coherent energy output. The VCSEL emits a narrow, more nearly circular beam than traditional edge emitters; this makes it easier to get the energy from the device into an optical fiber. Another interesting feature of VCSELs is its long lifetime, as there is no facet which can be damaged by high optical intensities.

The most common emission wavelengths of VCSELs are in the range of 750–980 nm (often around 850 nm), as obtained with the GaAs/AlGaAs material system. However, longer wavelengths of *e.g.* 1.3, 1.55 or even beyond 2 μm (as required for *e.g.* gas sensing) can be obtained with dilute nitrides (GaInNAs

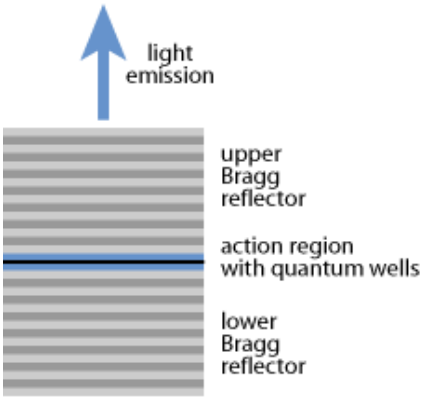

Figure 1.19: Schematic gain structure of a VCSEL

quantum wells on GaAs) and from devices based on indium phosphide (InAlGaAsP on InP) [27].

Frequency chirp Despite the advantages discussed so far, since the VCSEL is a semiconductor laser, when directly modulated, it experiences the frequency chirp: the time dependence of the instantaneous frequency of an optical pulse. A side effect of the power modulation is that the carrier density in the active region of a laser diode changes, and this leads to temporally varying phase changes, *i.e.*, to a chirp in the laser output. Whereas this is not seen when analyzing the optical power *vs.* time at the laser output, that chirp can have substantial effects when the data signal is transmitted through a standard single-mode fiber. Essentially, this is because the *chromatic dispersion* (see section 1.2), of the fiber means a frequency-dependent time delay, and this in conjunction with the chirp leads to signal degradation. These distortions are the main factors limiting the bit rate. In general, the laser chirp may be eliminated by applying the external modulator, or the dispersion may be compensated, or the transmission span may be divided by regenerators into the shorter ones [27].

Direct intensity modulation leads to some variation of the carrier concentration in the laser active region, what affects the refractive index and so frequency of a generated optical signal. Thus, the laser intensity modulation leads to (usually undesired) frequency chirp. The chirp of single-frequency laser may be described by the following equation:

$$\Delta\nu(t) = \frac{\alpha}{4\pi}\left(\frac{d}{dt}[\ln(P_L(t)) + \kappa P_L(t)]\right) \tag{1.28}$$

where $\Delta\nu(t)$ is the instantaneous frequency deviation, α is the so-called line enhancement factor, κ is the adiabatic chirp coefficient, and $P_L(t)$ is the laser output power [28].

Laser frequency chirp results in significant spectral broadening when the laser injection current is modulated; material and structural properties of the laser contribute to the resulting chirp [29].

This feature will be further investigated in Chapter 3, in section 3.2.3, and 3.3.2.

1.8 State of the art results

Several research groups demonstrated high transmission capacity in short-range reach over MMFs with VCSELs operating at 850 nm and modulation bandwidth of about 20 GHz (up to 24 GHz in [11]):

- By using 4-PAM modulation, transmission systems reach up to
  - 60 Gbit/s over 2 m [11]
  - 30 Gbit/s over 200 m [12]
  - 25 Gbit/s over 500 m [13].
- By using 16-QAM modulation format on a single subcarrier
  - 10 GBd over 200 m [15].
- By using DMT
  - 30 Gbit/s over 500 m [14]
  - 28 Gbit/s over 1 km [14].

850-nm wavelength represents the *"first spectral window"*, characterized by very high attenuation due to the *multimode dispersion* which limits the propagation to few meters (see section 1.2.2). DMT allows to propagate over a reach up to 1 km, since it confers robustness to multimode dispersion thanks to a reduced symbol rate with respect to single-carrier modulations, and loading algorithms (see sections 1.4 and 1.5)

Higher distances have been reached over SMFs, with VCSELs operating at 1550 nm. Apart of the 2,5 GHz VCSEL modulation bandwidth used in [7], the other results refer to a VCSEL modulation bandwidth from 10 GHz up to 20 GHz. Such systems reach up to:

- By using 4-PAM
  - 5 GBd over 5 km [9]
  - 25 GBd over 100 m [10].
- By using 4-QAM modulation format on a single subcarrier
  - 10 Gbit/s over 20 km [8].
- By using DMT
  - 12,5 Gbit/s over 20 km [7].

In 1550-nm wavelength, the *"third spectral window"*, the propagation along higher distances is possible since no multimode dispersion is present and the fiber attenuation is lower with respect to the *"first spectral window"*. However, propagation is affected by the *chromatic dispersion* (see section 1.2.1).

Therefore, the possibilities offered by FDM, which simplifies to the maximum extent the digital signal processing, in combination with multilevel modulation formats have not been plenty exploited so far: in literature have been proposed mainly single subcarrier solutions [8, 15]. This thesis presents FDM with multilevel modulation formats as transmission technique for a relatively short-range optical system. In order to reach distances of the order of few tens of kilometers, SMF is employed.

In Chapter 2, the strategy adopted in this thesis will be further investigated.

Chapter 2

Proposed solution

2.1 Architecture

VCSELs have several attractive properties such as large modulation bandwidth (up to about 24 GHz in [11]), low driving voltage, wavelength tunability, wafer-scale testing, easy packaging, and low carbon footprint. These advantages make VCSELs the favourite light source for high-speed and short range optical communication links using IM/DD technique. Optical links that use long-wavelength VCSELs and SMFs are limited in transmission reach by *chromatic dispersion* of optical fibers (see Chapter 1, section 1.2.1), combined to frequency chirping caused by direct modulation of the VCSEL (see Chapter 1, section 1.7), and large occupied bandwidth of signals [8].

Advanced modulation formats have been proposed in order to reduce the bandwidth of the signals: high-speed PAM for VCSELs has been demonstrated [9–13]. Its scalability is limited since it is a single-carrier modulation. OFDM, and in particular DMT, are promising technologies for both increasing spectral efficiency and dispersion tolerance by means of loading algorithms (see Chapter 1, section 1.5). High speed data transmission of DMT signal using VCSELs has been demonstrated recently [7, 14] . However, OFDM systems are affected by:

- High peak-to-average power ratio:

  OFDM and in particular DMT performance gets better for a large number of subcarriers. The most important reason is that with many subcarriers, the frequency-selective transmission channel can be better decomposed into

frequency-flat subchannels so that zero-forcing equalization at the demodulator can be more effective. The peak-to-average power ratio (PAPR) is the signal peak amplitude squared (giving the peak power) divided by the signal root mean square (rms) value squared (giving the average power). It is the square of the crest factor μ:

$$\text{PAPR} = \frac{|x|^2_{peak}}{x^2_{rms}} = \mu^2. \tag{2.1}$$

A high PAPR is therefore a direct consequence to the large crest factors which affect the modulation techniques with many subcarriers (OFDM and DMT), characterized by highly dynamic amplitude values. High PAPR is a detrimental aspect as it decreases the signal-to-quantization noise ratio (SQNR) of the analog-digital converter and digital-analog converter while degrading the efficiency of the power amplifier in the transmitter.

- High implementation complexity:

  the high speed digital signal processing (for example > 40 GS/s to reach capacities of the order of tens Gb/s) required for IFFT and FFT operations, could result in prohibitive costs. In a highly competitive market such as mass-consumer applications, the complexity (and therefore price) of such digital signal processing techniques should be well-chosen to optimize certain key factors such as price, energy-efficiency, ease of use, quality of service, transmission speed, novel application scenarios.

A simpler method exploited in this thesis is represented by FDM, in combination with multilevel modulation formats, which on the one hand meets the need for higher spectral efficiency with respect to the single-carrier modulations and provides dispersion tolerance compensation solutions (with loading algorithms), and on the other hand overcomes the typical OFDM disadvantages. This thesis presents therefore FDM as modulation format for a relatively short-range optical system which adopts IM/DD technique (with ODSB input signal), low-cost long-wavelength VCSEL and standard SMF; no optical amplifier is employed along the optic fiber path.

Figure 2.1, shows a conceptual system diagram of the IM/DD technique adopted in this thesis. A purely real signal is used to modulate the intensity of the light

emitted by the laser, so that only one DAC is required, and the direct detection results in the modulus squared of the input signal. The transmitted resulting signal is an ODSB one, which requires a simpler and cheaper system compared to that of SSB (see Chapter 1, section 1.6). After digital-to-analog conversion of the input baseband digital FDM signal and optical intensity modulation (with a VCSEL as light source), the resulting signal propagates along few tens of kilometers within SMF and it is finally directly detected by a photodiode to be then analog-to-digital converted.

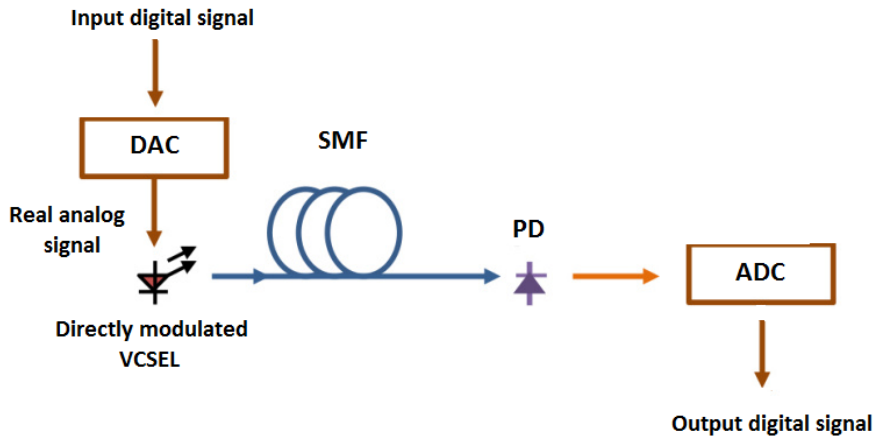

Figure 2.1: Conceptual system diagram

The goal of the work is to reach the highest possible capacity of the system with a minimum bit error rate less than 3.8×10^{-3} (for exploiting advanced forward error correction, FEC, with 7% overhead, see section 2.3.2) , at different fiber lengths. Following this approach, the number and the modulation order of subcarriers for maximizing FDM transmission performance over an optical IM/DD channel are investigated, by using bit and power loading (see section 2.2). It is shown that record bit-rates of up to 28 Gbit/s over 10 km SMF can be achieved, by using equalization (see Chapter 4).

2.2 Transmission strategy

This thesis exploits FDM technique to simplify to the maximum extent the digital signal processing in relatively short-range optical systems. In order to maximally increase the spectral efficiency, FDM is used in combination with multilevel modulation formats.

With FDM, in principle flexibility is present for each sub-band to employ a different modulation scheme. The strategy is therefore to employ the highest modulation rate possible.

Bit and power loading As already introduced in Chapter 1, section 1.5, bit loading and power loading are promising solutions in case of multicarrier transmission systems affected by *chromatic dispersion* (see Chapter 1, section 1.2.1), which introduces strong frequency selective fading (see Chapter 3, section 3.3.2). Moreover, bit and power loading let to achieve high volume of traffic by increasing the capacity of such systems, in which the limited bandwidth of some electrical components (as for example that of DACs and ADCs), can reduce the overall performance. Robustness against fiber dispersion and flexibility in the spectrum usage are obtained by allocating different number of bits and power to the subcarriers, according to the channel profile. The number of bits per subcarrier is allocated according to its corresponding signal-to-noise ratio (SNR): the (usually QAM, see Chapter 1, section 1.4.2) constellation size of each subcarrier is selected according to the number of bits that are allocated to it. Different loading techniques have been proposed in the literature; the most exploited are: *rate-adaptive* and *margin-adaptive*.

Rate-adaptive algorithms maximize the bit rate for a fixed bit-error ratio (BER) and given power constraint, while *margin-adaptive* algorithms minimize the BER for a fixed bit rate. The result is a large performance gain at relatively low complexity because such bit-loading algorithms only have to be computed during setup of a transmission link and not updated continuously. Until now, only *rate-adaptive* bit loading has found widespread use in commercial systems. The main advantage of *rate-adaptive* bit loading is that no matter how bad the transmission channel is, data transmission (even at very low bit-rates) is always possible. The *rate-adaptive* bit loading algorithm is a reformulation of the Shannon capacity formula and can be expressed as a problem of maximizing the total achievable bit-rate R in bit/s, which is the sum of the allocated bits per subcarrier b_n used for transmission given

by

$$\begin{aligned}\max_{P_n}(R) &= \max_{P_n}\Big(\frac{1}{N}\sum_{n=0}^{N-1} b_n\Big) \times B \\ &= \max_{P_n}\Big[\frac{1}{N}\sum_{n=0}^{N-1} \log_2\Big(1+\frac{SNR_n}{\Gamma}\Big)\Big] \times B \\ &= \max_{P_n}\Big[\frac{1}{N}\sum_{n=0}^{N-1} \log_2\Big(1+\frac{P_n g_n}{\Gamma}\Big)\Big] \times B,\end{aligned} \tag{2.2}$$

where B is the bandwidth of the signal, n is the subcarrier index, N is the total number of available subcarriers, $SNR_n = P_n \times g_n$ is the SNR per subcarrier, g_n represents the subcarrier SNR when unit power is applied, Γ is the difference (gap) between the SNR needed to achieve maximum (Shannon) capacity and the SNR to achieve this capacity at a given bit error probability, and P_n is the allocated power per subcarrier, subject to a power constraint given by

$$\sum_{n=1}^{N-1} P_n = P_{tot} \tag{2.3}$$

whereP_{tot} is the fixed total available power for transmission. The problem is now to find the optimum distribution of b_n, for $n = 0, 1, ..., N$, and the corresponding power distribution per subchannel P_n, in order to maximize the system bit-rate. Maximum bit-rate is not always achieved when all N subchannels are allocated with information bits, so that b_n and P_n can be 0 for some particular n. Therefore, the optimal solution is not always to use all available subchannels to transmit information, but to use only the ones with the highest SNR. The solution to this bit-rate maximization problem is based on the use of Lagrange multipliers and is given by

$$P_n + \frac{\Gamma}{g_n} = \text{constant}, \tag{2.4}$$

which is commonly known as *water-filling*. This equation states that the solution that maximizes bit-rate, under the constraint of 2.3, is the one where all the

subcarriers that are used to transmit information have a constant level $P_n + \frac{\Gamma}{g_n}$. The optimum solution is to distribute the total available transmission power P_{tot} to the subcarriers with the highest channel SNR represented by $\frac{g_n}{\Gamma}$, "just like filling a bathtub with water where water flows into the deepest point first" [2].

Water-filling algorithm starts by discarding the subcarriers that are least energy-efficient from information transmission, and redistributing the energy to more efficient subcarriers to support higher data rates. The non-integer number of allocated bits per subcarrier are then rounded to the nearest integer and the corresponding energy is in- or decreased to support the newly-allocated number of bits at the same performance [22].

In this thesis, these principles are empirically employed to choose the proper modulation rate of each subcarrier, considering its corresponding frequency range on the system transfer function (TF) and the effects of the frequency fading due to transmission (see Chapter 3, section 3.3.2).

Moreover, in order to optimize the allocation of the subcarriers, additional expedients are investigated:

- To best use the system spectrum, the subcarriers will be put adjacent and equally spaced.
- A Nyquist pulse shaping with roll-off factor = 0 (in order to minimize the bandwidth occupancy), will be employed.
- For limiting the PAPR, the number of subcarriers has to be reduced; a good trade-off is to use 1 GHz bandwidth for each subcarrier.
- Electronic subcarriers pre-equalization is employed by means of $\mathrm{TF}^{-1/2}$, so that the power results equally distributed as much as possible.

Nyquist pulse shaping Since the communication channel has a frequency-dependent spectrum (see Chapter 3, section 3.3.2), dispersion arises and *inter-symbol interference* (ISI) affects the transmission.

In practice, *Nyquist's criterion*:

$$\sum_n P\left(f - \frac{n}{T_b}\right) = T_b \tag{2.5}$$

is applied to baseband filtering, so that symbols can be transmitted over the channel within a limited frequency band, without ISI.

The most widely used Nyquist filters follow the raised cosine (RC) frequency response defined by:

$$G_{RC}(f) = \begin{cases} 1, & 0 \leq f \leq B(1-\alpha) \\ \frac{1}{2}\left\{1 + \cos\left[\frac{n}{2B\alpha}(f - B(1-\alpha))\right]\right\}, & B(1-\alpha) < f \leq B(1+\alpha) \\ 0, & B(1+\alpha) < f \end{cases} \tag{2.6}$$

where B is the single-sided filter bandwidth corresponding to $\frac{1}{2T}$, and α is the *excess bandwidth* parameter usually called *roll-off factor*. The lower the roll-off factor, the narrower is the occupied bandwidth of the signal [30].

A Nyquist pulse shaping with roll-off factor = 0 is therefore employed in this thesis.

2.3 Receiver

In order to reach the highest possible capacity of the system at different fiber lengths, equalization techniques at the receiver side result necessary. The required minimum received BER is set to 3.8×10^{-3}, for exploiting advanced FEC with 7% overhead (see section 2.3.2).

2.3.1 Equalization

During propagation through SMFs, signal is mainly affected by *chromatic dispersion*, which introduces distortion. Dispersion compensation results therefore mandatory in a high-performance transmission system.

Electronic dispersion compensation allows accurate management of the dispersion and low costs. The most diffused electronic post-compensators (EPCs), at the receiver, is Feed Forward/Decision Feedback Equalizer (FFE/DFE). The purpose is to compensate the dispersion via digital filtering of the received signal.

The electrical current after detection can be written as:

$$c(t) = R_p \sum b_j g_j(t - jT) + n(t) \tag{2.7}$$

where b_j=0,1 is the transmitted bit, $g_j(t - jT)$ is the received pulse, whose shape depends on the position in the bit stream due to the presence of dispersion, T is the bit interval. Assuming $f(t)$ the pulse received in absence of distortion and neglecting the pulse shape dependence on the position in the bit stream, the distortion equivalent filter $D_\omega(\omega)$ is a filter able to transform the ideal pulse into the real one, that is:

$$g(t) = \int f(\tau) D(t - \tau) d\tau \tag{2.8}$$

where $D(t)$ is the IFT of $D_\omega(\omega)$. Therefore, once $D_\omega(\omega)$ is introduced, the distortion can be in principle compensated by inverting $D_\omega(\omega)$. Sampling at the Nyquist rate and truncating the series to a finite number, the FFE compensation algorithm results:

$$c_c(v) = R_p \sum_j b_j \left\{ \sum_{k=1}^{m} g_j(v - k - jT) d(k) + \sum_{k=1}^{m} n(v - k) d(k) \right\} \tag{2.9}$$

where $d(k)$ are the coefficients of the FFE filter.

Since the number of taps is finite, FFE does not assure a good chromatic dispersion compensation. In order to improve the performance, the FFE is usually complemented with a DFE, that is basically another set of delay lines and taps put as a feedback to the FFE.

High performance FFE/DFE relies on the choice of the coefficients, and many FFE/DFE use a least mean square (LMS) algorithm, which minimizes the mean squared error signal, to adapt the coefficients on the grounds of the receiver performances [31].

In practice, a "standard" equalizer commonly uses nine taps in the FFE and four in the DFE: this is the case in this thesis.

2.3.2 Forward error correction

Forward error correction (FEC) is a way to expand available bandwidth and improve the quality of transmission over noisy channels: it adds redundant information to a data stream, so enabling a receiver to identify and correct errors without the need for retransmission. As a consequence, there are several system improvements, such as extended range, higher data rate, greater power efficiency, increased data reliability.

The original user data to be transmitted over the channel is called *information bits*, while the data after the addition of error-correction information is called *coded bits*. For k information bits, the encoding process results in n coded bits, where $n > k$. All n bits are transmitted; at the receiver, these n bits are estimated. An FEC decoder utilizes the n bit estimated, along with knowledge of how all n bits were created, to generate estimates of the k information bits. The decoding process effectively detects and corrects errors in the n-channel bit estimates while recovering the original k information bits.

Since the flow of data is always moving forward (no retransmissions are requested), the process is called *"forward error correction"*.

FEC codes can be of three different types:

- convolutional
- block
- Turbo Codes

In a simple *convolutional* encoder, a sequence of information bits passes through a shift register, and two output bits are generated per information bit. Then, the two output bits are transmitted: the decoder estimates the state of the encoder for each set of two channel symbols it receives.

Block codes generate one or more *parity* bits from k information bits. These parity bits are appended to the information bits, resulting in a group of n bits where n > k. The encoded pattern of n bits is referred to as a code word, and this code word is entirely transmitted. Block decoders are usually rich in algebraic structure that can be used to facilitate decoding. The most popular block codes are Reed Solomon codes; another classical example of block codes is BCH.

Turbo Codes are very powerful codes. Starting from two or less constituent codes, which could be either convolutional or block type, data are encoded once

via encoder 1 and, after being scrambled, via encoder 2. The twice-encoded bits are then transmitted. At the receiver, decoding proceeds in the reverse order of the encoding process. The second decoder addresses errors left from the first; in order to maximize performance, this decoding process is typically iterated several times. Turbo Codes significantly increase the complexity of the decoders. The fact that one decoder's output feeds the input to the next decoder is analogous to a turbocharger in a high-performance engine: this is where the term "turbo " comes from [32].

The oldest FEC codes are able to provide error corrections with a received BER of the order of 10^{-6}; Reed Solomon codes require a 10^{-3} BER order, while Turbo Codes improve the transmission quality with a BER of the order of just 10^{-2}.

If the "two interleaved extended BCH(1020,988) super FEC code" is employed with a 10 times iterative decoding, performance can be improved, obtaining, *e.g.*, an output BER even less than 10^{-16} for an input BER equal to 4.00×10^{-3}. This technique adds slightly less than 7% overhead for the FEC bytes (this means that the data rate has to increase by 7% in order to transmit both the data and the FEC), providing a net coding gain better than 8,5 dB at BER 10^{-13}, with a 10 times iterative decoding [33].

In high-speed optical networks, a 6 dB gain is already a very significant performance improvement (approximately quadrupling the distance between regenerators, if present) [34].

In Chapter 3 the main devices employed in the proposed system will be characterized.

Chapter 3

Components characterization

3.1 System setup

In order to realize the highest possible capacity transmission over different single-mode fiber lengths, many system parameters have to be investigated and optimized. For this, the experimental setup depicted in Figure 3.1 is employed.

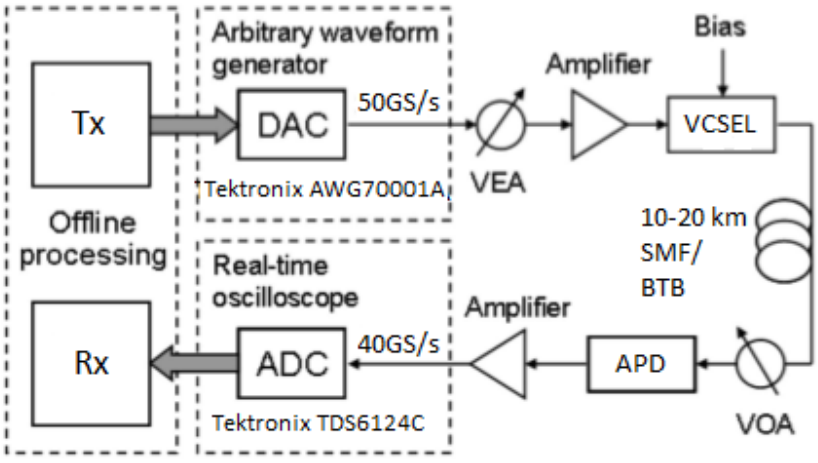

Figure 3.1: Experimental setup: Arbitrary waveform generator (AWG), single mode fiber (SMF), variable optical attenuator (VOA), avalanche photo-detector (APD), digital storage oscilloscope (DSO)

Using an arbitrary waveform generator (AWG), Tektronix AWG70001A, with a bandwidth of 12-14 GHz, a 1580-nm VCSEL is directly modulated (through an electrical variable attenuator and amplifier), at a sampling rate of 50 GS/s. The VCSEL has an electrical signal modulation bandwidth of approximately 5-6 GHz. The resulting intensity-modulated optical signal is then transmitted over different SMF lengths (10 km and 20 km), or directly coupled to the variable optical attenuator (VOA) in the back-to-back measurement case (BTB). Therefore, the received optical signal is detected by an avalanche photo-detector (APD); the resulting received electrical signal is then amplified and captured using a 12-GHz real-time Tektronix TDS6124C digital storage oscilloscope (DSO) running at a sampling rate of 40 GS/s for demodulation and evaluation. The FDM signal is generated using Matlab and then transmitted to the AWG; at the receiver side, after analog-to-digital conversion by means of the DSO, the signal post processing is implemented offline again via Matlab. This also includes evaluation of the BER transmission performance parameter per subcarrier, and the FFE/DFE equalization (see Chapter 2, section 2.3.1).

3.2 Source characterization

3.2.1 P vs I curve

Taking into account the IM/DD channel model presented in Chapter 1, section 1.3, Figure 3.2 shows the characteristic of the 1580-nm VCSEL employed in this thesis. The threshold value I_{th} is approximately 2,5 mA and the I_{bias} is 9,5 mA (within the linear region). The saturation effect starts at approximately 17 mA determining a maximum emission power P_{max} of 0,75 mW.

3.2.2 VCSEL electro-optic bandwidth

In order to evaluate the VCSEL electro-optic (E/O) bandwidth, a baseband OOK signal is transmitted to the system shown in Figure 3.1, in the BTB measurement case. The I_{bias} is set at 9,5 mA (according to section 3.2.1), and the AWG peak-to-peak voltage (V_{pp}) at 300 mV, which represents the best trade-off between amplitude peak and noise constraints. The performance evaluation is computed considering the direct detected BER (without equalization).

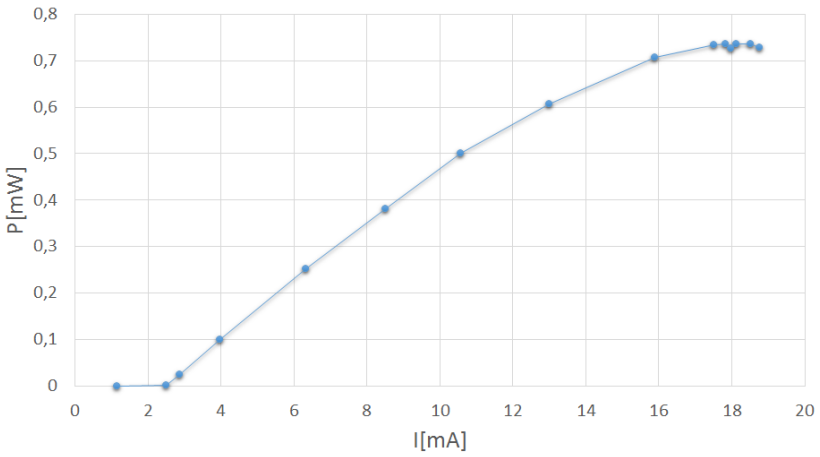

Figure 3.2: P vs I curve

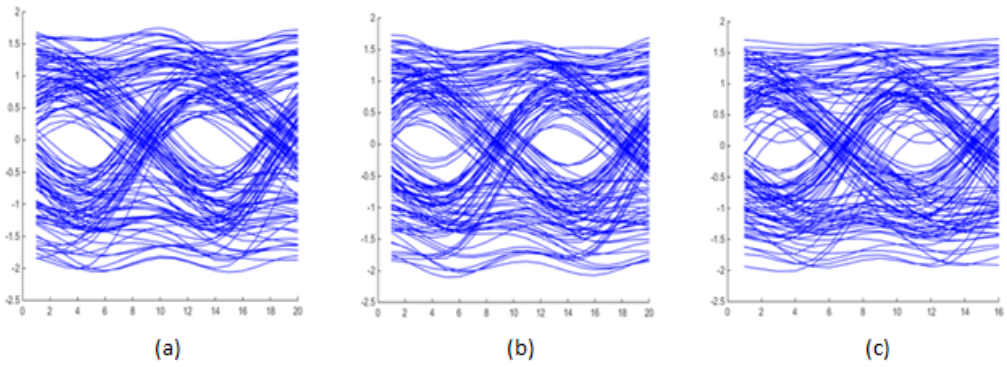

Figure 3.3: Eye diagrams at different capacities, BTB: (a) 8 Gbit/s; (b) 9 Gbit/s; (c) 10 Gbit/s

Figure 3.3 shows the eye diagrams relative to a direct detected BER less than 10^-6 (error free) for a 8 Gbit/s transmission up to -18 dBm (a), and for a 9 Gbit/s transmission up to -11 dBm (b). When 10 Gbit/s are transmitted, the direct detected BER is about 10^-2 (c). These results suggest an estimation VCSEL E/O bandwidth of about 5-6 GHz: much less than most of the VCSELs used in the literature experiments mentioned in Chapter 1, section 1.8. Apart of the 2,5 GHz VCSEL E/O bandwidth used in [7], the modulation bandwidth of the VCSELs employed usually starts from 10 GHz [8], up to 24 GHz [11].

3.2.3 Laser linewidth

In order to characterize the linewidth of a laser, different techniques can be adopted. The following sections present the theory related to this characterization, and the linewidth measurement of the VCSEL employed in this thesis.

Linewidth characterization

Laser linewidth is the width of the power spectral density of the emitted electric field in terms of frequency, or wavelength. The linewidth of a laser is strongly related to the temporal coherence, characterized by the coherence time or coherence length [27].

The *coherence time*, τ_c, is a measure of the spectral purity of the laser over time. It varies inversely with laser linewidth, $\Delta\nu$:

$$\tau_c = \frac{1}{\pi\Delta\nu}. \tag{3.1}$$

Defining the *velocity of light*, v_g, as:

$$v_g = \frac{c}{n_g} \tag{3.2}$$

where c is the speed of light in vacuum $\approx 3 \times 10^8$ m/s, and n_g is the group velocity index $\approx$ 1,47, the *coherence length*, L_g can be defined as:

$$L_g = v_g \times \tau_c. \tag{3.3}$$

The linewidth of a typical single-frequency semiconductor laser is of the order of 10 MHz. The two dominant causes of spectral broadening in single-longitudinal mode lasers are *phase noise* and *frequency chirp*. Random *phase noise* is created when spontaneous emission, originating in the laser cavity gain media, changes the phase of the freerunning laser frequency. Laser *frequency chirp* (see Chapter 1, section 1.7, and Chapter 3, section 3.3.2), results in significant spectral broadening when the laser injection current is modulated. The laser spectrum can be broadened well beyond the freerunning optical linewidth. Material and structural properties of the laser contribute to the resulting chirp, which represents in most cases an unwanted frequency modulation. Grating-based optical spectrum analyzers (OSAs) don' t offer the measurement resolution required for laser linewidth measurement, so alternative characterization methods must be used. They all require the following measurement assumptions:

- The laser is assumed to operate in a single-longitudinal mode (SLM).
- Typical laser lineshape: Lorentzian central peak, small sidebands.
- Between the interfering beams: polarization alignment and spatial overlap.
- SMF is employed.

A laser linewidth can be measured with a variety of techniques:

- *Heterodyne using a local oscillator*
- *Delayed self-heterodyne*
- *Delayed self-homodyne*

Heterodyne and *Self-homodyne* are two kinds of interference between two optical fields.

In particular, *Heterodyne* is the interference between two different fields. A local oscillator laser is used as a measurement reference to detect a second signal source with unknown spectral characteristics, as shown in Figure 3.4.

Two optical fields incise on the photodiode:

$$E_S(t) = \sqrt{P_S(t)} e^{i(2\pi\nu_S t + \phi_S(t))} \tag{3.4}$$

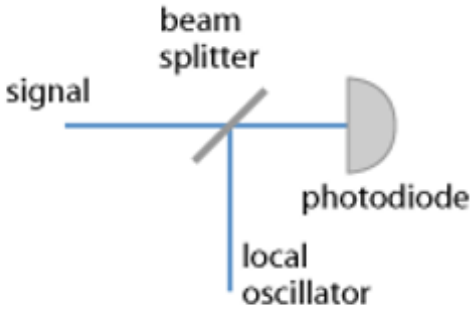

Figure 3.4: Setup for optical heterodyne detection.

$$E_{LO}(t) = \sqrt{P_{LO}(t)}e^{i(2\pi\nu_{LO}t+\phi_{LO}(t))} \tag{3.5}$$

where ϕ is optical phase which takes into account any phase noise. The interference between the two waves causes intensity variations that are detectable using a photodiode:

$$E_T(t) = E_S(t) + E_{LO}(t) \tag{3.6}$$

Since the power detected is:

$$P(t) = |E_T(t)|^2, \tag{3.7}$$

the photocurrent generated in the detector is:

$$i(t) = R|E_T(t)|^2 \tag{3.8}$$

where R is the detector responsivity:

$$R = \frac{\eta dq}{hf} \tag{3.9}$$

with ηd the detector quantum efficiency ($0 < \eta d \leq 1$), q the electronic charge, and

hf the photon energy. Therefore it has:

$$i(t) = R[P_S(t) + P_{LO} + 2\sqrt{P_S(t)P_{LO}}\cos(2\pi f_{IF}t + \Delta\phi(t))] \tag{3.10}$$

where $\Delta\phi(t) = \phi_S(t) - \phi_{LO}(t)$.

The first two terms correspond to the direct intensity detection, the third term is the important heterodyne mixing term. The actual optical frequency is gone and only the difference $f_{IF} = f_S - f_{LO}$ remains. If either field were separately detected on the photodiode, the resulting photocurrent would follow only the power variations $P(t)$ and all phase information would be lost.

Self-homodyne is the interference between a field and a delayed replica: one of the two interfering optical fields is a delayed version of the other. This condition can be created by a variety of two-path optical circuits such as the Mach-Zehnder, Michelson, and Fabry-Perot interferometers, as shown in Figure 3.5. Important issue is that the interferometer delay τ_0 remains smaller than the source coherence time τ_c. In this case we have:

$$i(t) = R[P_1(t) + P_2(t) + 2\sqrt{P_1P_2}\cos(2\pi f_0\tau_0 + \Delta\phi(t, \tau_0))] \tag{3.11}$$

where $\Delta\phi(t, \tau_0) = \phi(t) - \phi(t - \tau_0)$ [29].

Linewidth measurement

The technique employed in this thesis to measure the laser linewidth is *delayed self-homodyne*. It is a very simple means which offers extremely high resolution. The optical circuit must deliver to the photodetector two fields, one being a delayed replica of the other. The mixing process can be analyzed with an electrical spectrum analyzer (ESA).

Self-homodyne can be described mathematically as a single-delay autocorrelation. The optical spectrum at f_o autocorrelates with the delayed version of itself to produce a time-fluctuating spectrum centred at 0 Hz. The convolution originates from the multiplication of the time-varying local oscillator field with the signal field in the photodetector. Multiplication in the time-domain is equivalent to convolution in the frequency domain [35].

For the case of Lorentzian lineshape, the autocorrelation function is also Lorent-

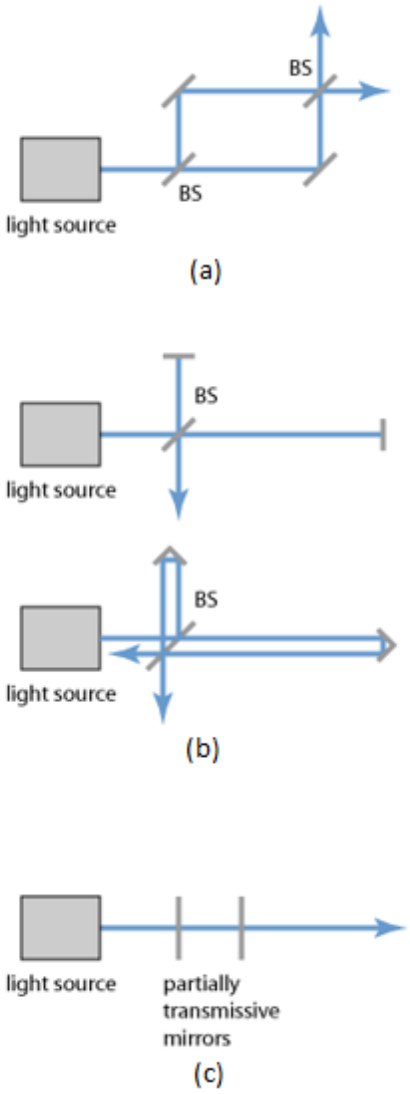

Figure 3.5: Homodyne detection:(a) Mach–Zehnder interferometer; (b) Michelson interferometers; (c) Fabry–Pérot interferometer.

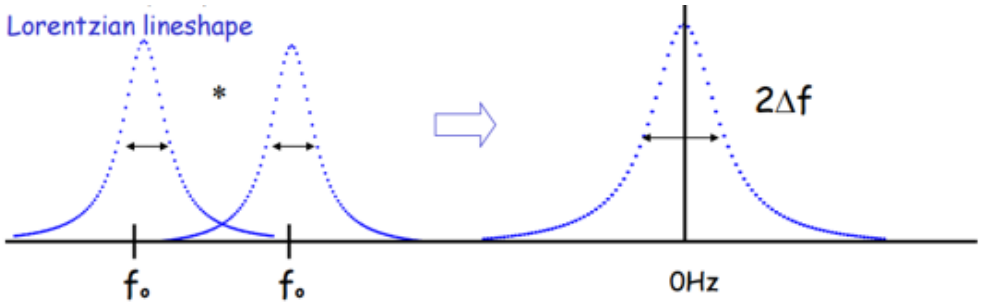

Figure 3.6: Delayed self-homodyne spectrum

zian and it has a linewidth exactly twice that of the original lineshape. Since the mixing term is the test-laser spectrum convolved with itself, the displayed lineshape will always be symmetrical. The *delayed self-homodyne* method centers the mixing spectrum at 0 Hz, therefore only half of the symmetrical spectrum is viewed, as shown in Figure 3.6.

If:

$$\tau_0 \geq \frac{1}{\Delta\nu}, \tag{3.12}$$

the mixing becomes independent on the phases of the interfering light, leading to a more stable measurement: *incoherent mixing*.

The photocurrent spectrum can be written as:

$$S_i(f) \approx R^2\{S_d(f) + 2[S_s(f) \otimes S_s(-f)]\}. \tag{3.13}$$

For large $\Delta\nu \times \tau_0$, the frequency resolution is determined by the linewidth of the test laser. In the other extreme, when that product becomes small compared to unity, the resolution is limited by the differential time delay of the interferometer [29].

Figure 3.7 shows the employed 1580-nm VCSEL linewidth measurement, by means of *delayed self-homodyne* technique, at -10 dBm evaluation power. At 9,5 mA (I_{bias}, according to section 3.2.1), the laser experiences approximately 6 MHz linewidth.

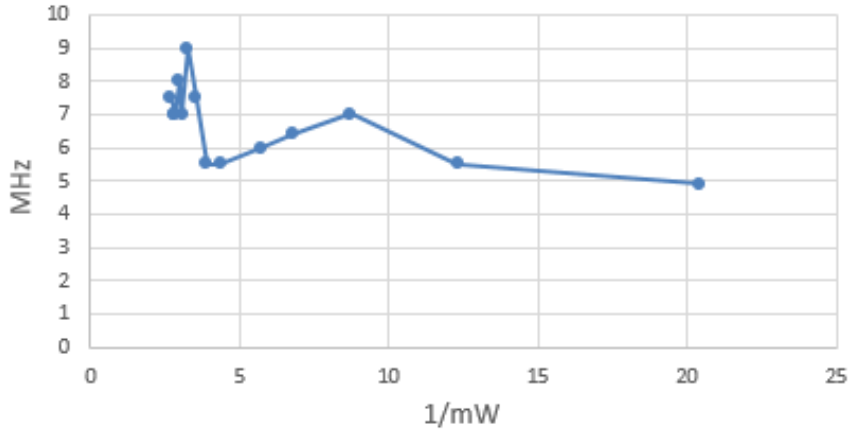

Figure 3.7: 1580-nm VCSEL linewidth

3.3 System Transfer Function estimation

3.3.1 Transfer Function: arbitrary waveform generator

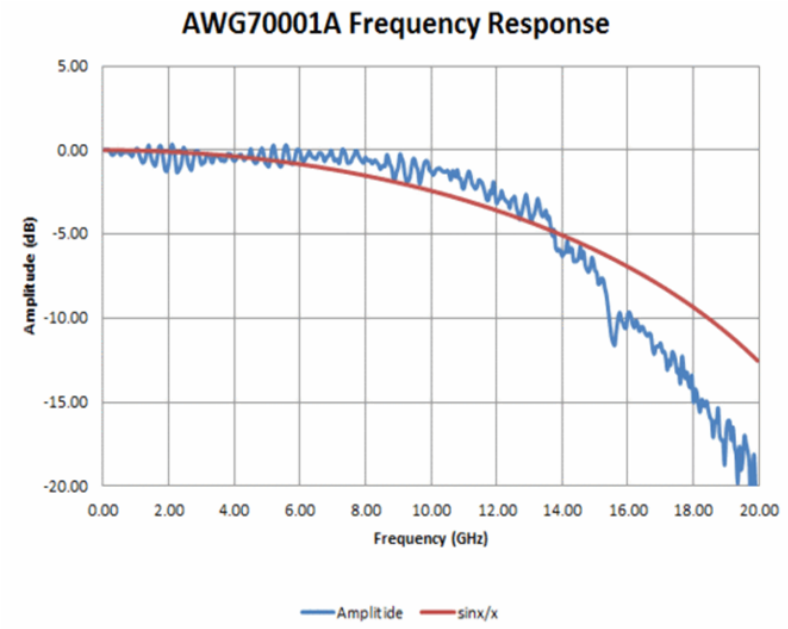

Figure 3.8: AWG 70001A Frequency Response

Figure 3.8 is directly from the AWG70000 series data sheet [36] and it shows in red the true $\sin(x)/x$ response. The AWG frequency response is characterized by many ripples (amplitude in blue), due to the slight impedance mismatching between the two interleaved DACs used to achieve 50 GS/s sample rates (25 GS/s each DAC), as shown in Figure 3.9.

DAC interleaving consists of using two or more DACs working at a nominal sample rate to generate a signal as if it were created by a higher sample rate device.

As shown in the AWG frequency response in Figure 3.8, the ripples maximum peak-to-peak is about 1 dB, and the electrical bandwidth can be estimated around 12-14 GHz.

3.3.2 Total Transfer Function

Figure 3.10 shows the frequency response of the system in Figure 3.1 to a sinusoidal pulse. The blue line represents the BTB measurement case, the green

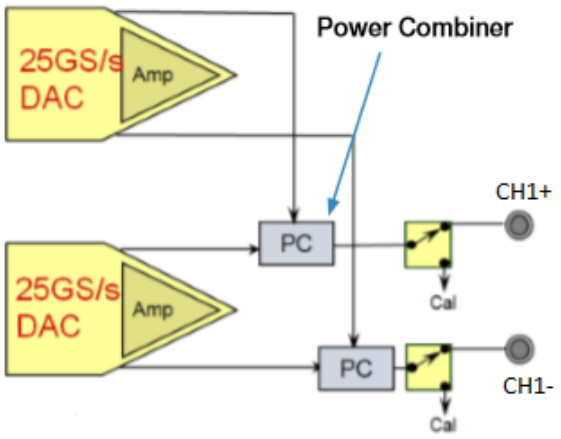

Figure 3.9: DAC Interleaving

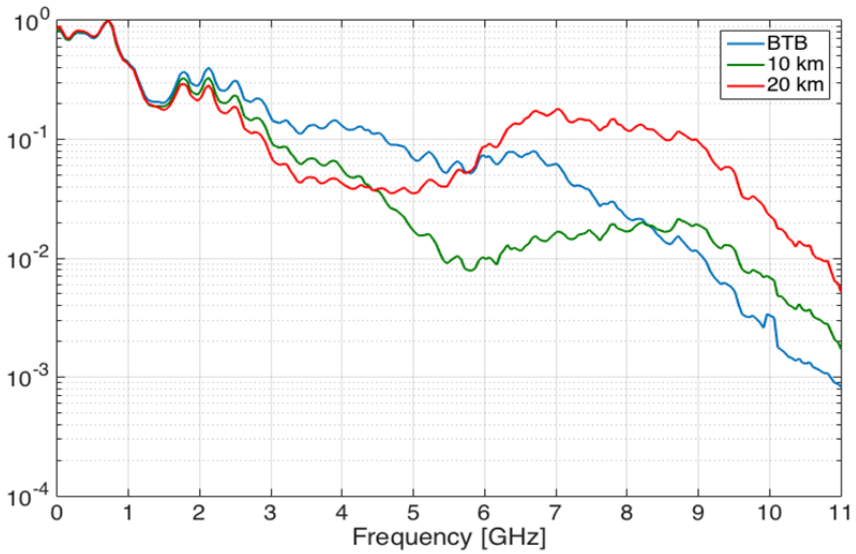

Figure 3.10: Total Transfer Function

line represents the system frequency response over 10 km SMF, and the red line represents the system frequency response over 20 km SMF. The total tranfer function (TF) is therefore affected by the spectral content of each component of the system:

- AWG: 12-14 GHz bandwidth.
- Electrical driver: 12 GHz bandwidth.
- VCSEL: 5-6 GHz bandwidth.
- SMF chromatic dispersion (see Chapter 1, section 1.2.1).
- APD: 7,5 GHz bandwidth.
- Electrical amplifier: 15 GHz bandwidth.
- DSO: 12 GHz bandwidth.

Unlike the BTB measurement case, which presents a slight frequency dip around 5-6 GHz, the transmission over 10 km SMF seems to be damaged by a deeper frequency dip around 6 GHz, whereas over 20 km SMF the frequency dip seems to be shifted around 4 GHz.

In order to investigate the effects of the SMF chromatic dispersion on the system frequency response, the *small signal* theory is employed in the next section.

Impact of chromatic dispersion

Since the information is transmitted by means of an intensity modulation (see Chapter 1, section 1.6), the modulated optical signal is an ODSB one, as depicted in Figure 3.11.

Figure 3.11: IMDD signal E/O spectrum in the electrical and optical domains

Due to chromatic dispersion, the modulation sidebands of the signal and the optical carrier will propagate with different velocities in the fiber and each frequency

of the signal will experience a particular phase variation. As a consequence, at certain frequencies, the chromatic $dispersion \times fiber$ length product will cause the two modulation sidebands to be in counter phase, thereby producing a dip in the amplitude of the channel's frequency response and thus characterizing a frequency-selective channel [37].

Moreover, also the VCSEL experiences the frequency chirp when directly modulated: intensity modulation affects the carrier concentration in the laser active region, as already explained in Chapter 1, section 1.7. In this thesis, dispersion compensation techniques or regenerators are not adopted, since they are not suitable solutions for low cost short-range transmission applications.

The dispersion induced frequency fading of the IM/DD channel constitutes the main limitation when increasing the transmission range.

Many mathematical models addressing the IM/DD channel have been proposed in literature. The vast majority of them focus the analysis on the *small-signal regime (SSR)*.

The *small signal* analysis implies that the average intensity $\langle S \rangle$ is larger then the noise or modulation term $\Delta S_{in}(t)$. The small signal theory implies also that the frequency modulation or noise $\phi_{in}(t)$ is small enough, yielding that $\Delta S_{in}(t)$, $\phi_{in}(t)$ and their derivatives may be neglected. This requires a small intensity and frequency modulation index [38].

Using this model, the small signal power modulation transfer function $H_F(f)$ between intensity modulation at the fibre input and output can be written as:

$$H_F(f) = \cos\theta_D - H_{PM}(f)\sin\theta_D \tag{3.14}$$

where f is the modulation frequency, $H_{PM}(f)$ is the ratio between the phase modulation (PM) depth and the amplitude modulation (AM) index at the fibre input. When propagating along the fibre, the sidebands are phase shifted $\theta_D = \pi(f/f_D)^2$ relative to the carrier, where $f_D^2 = c/(\lambda^2 \times DL)$. c is the speed of light, λ the wavelength, D the dispersion coefficient, and L is the fibre length.

For a directly modulated semiconductor laser transmitter:

$$H_{PM}(f) = \alpha - j\alpha f_c/f \tag{3.15}$$

where α is the linewidth enhancement factor, and f_c is the frequency at which the *adiabatic* and *transient chirp* have the same magnitude. α represents the laser' s effective amplitude-phase coupling factor. A large value of α results in increased laser linewidth and chirp (see section 3.2.3). α can be seen also as the link between power changes in the laser cavity to phase changes of the emitted light [39].

The transfer function of the dispersive channel is therefore related to the chirp of the optical signal generated by the directly modulated laser:

$$\Delta\nu(t) = \frac{\alpha}{4\pi}\left(\frac{1}{P(t)}\frac{dP(t)}{dt} + \kappa P(t)\right) \tag{3.16}$$

where $\Delta\nu(t)$ is the instantaneous frequency deviation, α is the linewidth enhancement factor, κ is the adiabatic chirp coefficient, and $P(t)$ is the laser output power. The first term in the above equation, proportional to derivative of the output power is called the *transient chirp*, and the second, directly proportional to the power, is the *adiabatic chirp* [28].

Frequency fading due to dispersion estimation

In Figure 3.12 and Figure 3.13, the frequency fading which affects the transmission respectively over 10 km and 20 km SMF is estimated.

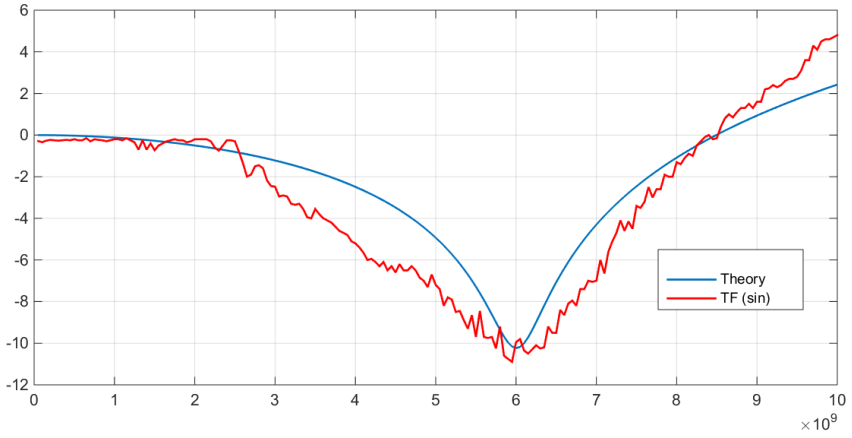

Figure 3.12: Frequency fading estimation over 10 km SMF

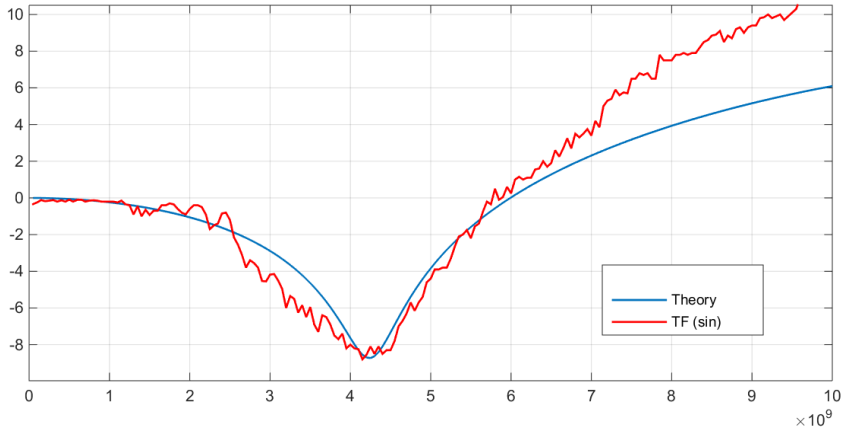

Figure 3.13: Frequency fading estimation over 20 km SMF

The blue lines in Figure 3.12 and Figure 3.13 show the system frequency response following the *small signal* model presented in the previous section, over 10 km SMF and over 20 km SMF respectively. The red lines represent the system frequency response to a sinusoidal pulse, over 10 km SMF and over 20 km SMF.

The frequency fading results therefore in a frequency dip around 6 GHz in the 10 km single-mode fiber case, Figure 3.12, and around 4 GHz in the 20 km single-mode fiber case, Figure 3.13. The *small signal* model and the sinusoidal pulse show basically the same depth of the frequency dips, but the sinusoidal pulse shows a higher mignification of the frequencies above the dips with respect to the *small signal* model.

By using the *small signal* model (equations 3.14 and 3.15), the frequency fading at different transmission lengths can be estimated, as depicted in Figure 3.14. The parameters adopted for the estimation are the following:

- λ = 1579.8 nm
- D = 19 ps/nmkm
- α = 5.5
- $f_c = \frac{\kappa P}{2\pi}$ = 580 MHz.

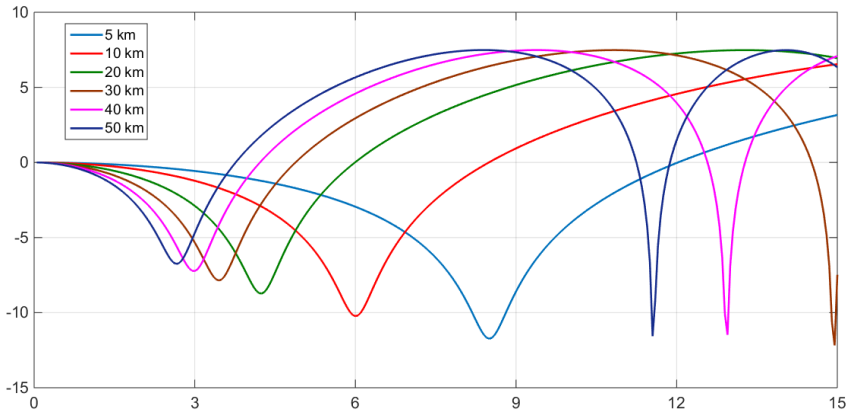

Figure 3.14: Frequency fading estimation: after 5 km, 10 km, 20 km, 30 km, 40 km, 50 km.

Chapter 4 will present the experimental activity and its results.

Chapter 4

Experimental activity

4.1 Experimentation

As already depicted in Chapter 3, section 3.1, the setup shown in Figure 4.1 is employed for the experimental activity to demonstrate the operation of an optical system with a target net capacity of 25 Gb/s over tens km reach.

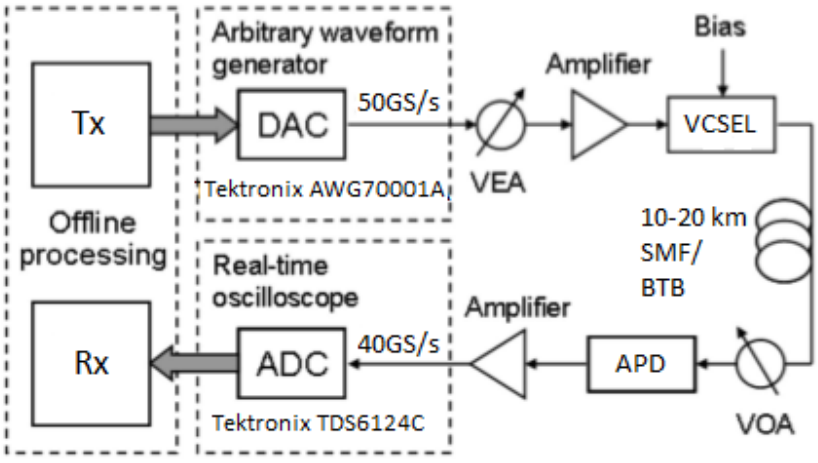

Figure 4.1: Experimental setup: Arbitrary waveform generator (AWG), single mode fiber (SMF), variable optical attenuator (VOA), avalanche photo-detector (APD), digital storage oscilloscope (DSO)

Following the techniques discussed in Chapter 2, section 2.2, as concerning the modulation order of the FDM subcarriers and their allocation by means of bit and power loading, Nyquist pulse shaping with roll off 0, and electronic pre-equalization (by means of $TF^{-1/2}$), the experimental transmission is managed, with particular care for the spectrum usage to limit the peak-to-average power ratio (1 GHz bandwidth is used for each sub-band). At the receiver side, equalization techniques (FFE/FDE, with 2 samples per bit, nine taps in the FFE, and four taps in the DFE), are employed in order to compensate the chromatic dispersion (see Chapter 1, section 1.2.1), so maximizing the capacity results. Target BER is set to 3.8×10^{-3}, for exploiting advanced FEC with 7% overhead (see Chapter 2, section 2.3.2).

According to Chapter 3, section 3.2.1, VCSEL I_{bias} is set to 9,5 mA during the experimental measurements, so ensuring to work within the linearity condition. Another important operating parameter common to all the measurements, is the AWG peak to peak voltage, V_{pp}, set to 300 mV: it is a trade off between the need for amplitude (of the subcarriers), and the noise constraints. In order to further improve the transmission quality, also a proper amplitude for each sub-band is investigated, according to the system total TF (see Chapter 3, section 3.3.2).

In order to reduce the $carrier \times subcarriers$ interference (see Chapter 1, section 1.6.2), a frequency guard band is maintained by allocating the first sub-band slightly distant from the optical carrier. This requirement is realized centering the first subcarrier at 0,75 GHz of the available spectrum (see Chapter 3, section 3.3.2). The spectrum is limited to about 10 GHz by the system components.

The experimental activity is therefore handled at different fiber lengths (BTB, 10 km, 20 km), with the aim to reach the highest possible capacity of the system within the fixed 3.8×10^{-3} target BER for each subcarrier. Record bit-rate of up to 28 Gb/s over 10 km SMF is shown.

4.2 Back-to-back performance

In the BTB measurement case, the maximum measured transmission power of the system is - 5,4 dBm. No chromatic dispersion affects the propagation, since no optical fiber is present. However, the total transfer function of the system (see Chapter 3, section 3.3.2), reported in Figure 4.2, must be considered in order to choose the proper modulation order of each frequency sub-band.

The modulation order of the subcarriers can be maximized to 16-QAM (with a correspondent bit rate of 4 Gb/s), until the total transfer function shows an attenuation of the frequencies above 7 GHz, due to the spectral content of each component of the system which limits the spectrum. To the latest portion of the spectrum a 4-QAM modulation order is therefore assigned (with a correspondent bit rate of 2 Gb/s). The latest subcarrier within the available spectrum is centered at 9,75 GHz.

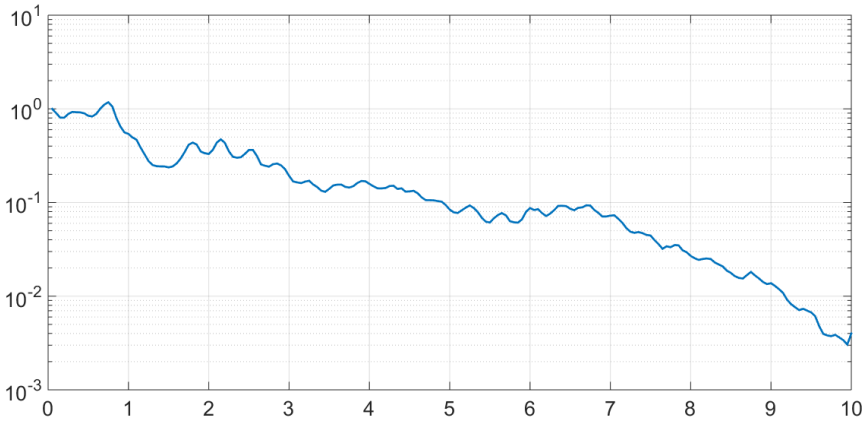

Figure 4.2: Total transfer function in the back-to-back measurement case

Figure 4.3, shows the details of such FDM modulation, with the number and modulation order of the subcarriers employed for maximizing the BTB transmission performance, and their relative BER. As said before, the first sub-band is allocated at 0,75 GHz, in order to obtain a frequency guard band able to reduce the $carrier \times subcarriers$ interference. Taking into account 10 equally-spaced subcarriers modulated at 1 GBd, bit rate of up 34 Gb/s is achieved. The results refer to a transmission power of -8 dBm, nearer than the maximum -5,4 dBm to the power at which the measurements over 10 km SMF and 20 km SMF are handled (see section 4.3 and section 4.4).

Figure 4.4 and Figure 4.5 show respectively the generated (with electronic pre-equalization by means of $TF^{-1/2}$) and received spectra related to the 34 Gb/s BTB transmission.

Figure 4.6(a) and Figure 4.6(b) show respectively an example of generated and received eye diagram (related to the 34 Gb/s BTB transmission), in case of 16-QAM modulation of the subcarrier at 3,75 GHz, while Figure 4.6(c) and Figure

16QAM @ 0.75 GHz bit rate: 4Gbps	16QAM @ 1.75 GHz bit rate: 4Gbps	16QAM @ 2.75 GHz bit rate: 4Gbps	16QAM @ 3.75 GHz bit rate: 4Gbps	16QAM @ 4.75 GHz bit rate: 4Gbps	16QAM @ 5.75 GHz bit rate: 4Gbps	16QAM @ 6.75 GHz bit rate: 4Gbps	4QAM @ 7.75 GHz bit rate: 2Gbps	4QAM @ 8.75 GHz bit rate: 2Gbps	4QAM @ 9.75 GHz bit rate: 2Gbps
BER_eq: 5E-04	BER_eq: 1E-03	BER_eq: 9.6E-04	BER_eq: 1.3E-03	BER_eq: 1.3E-03	BER_eq: 7E-04	BER_eq: 9.7E-04	BER_eq: 2E-03	BER_eq: 1.1E-03	BER_eq: 2.5E-03

Figure 4.3: 34 Gb/s BTB.

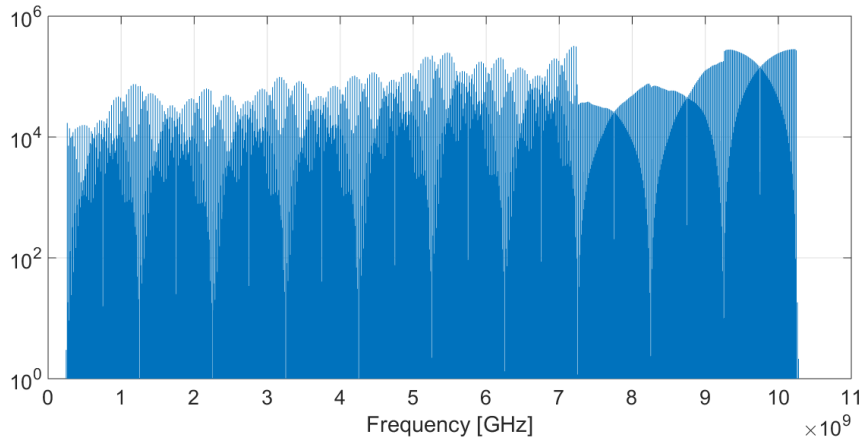

Figure 4.4: Generated spectra: 34 Gb/s BTB.

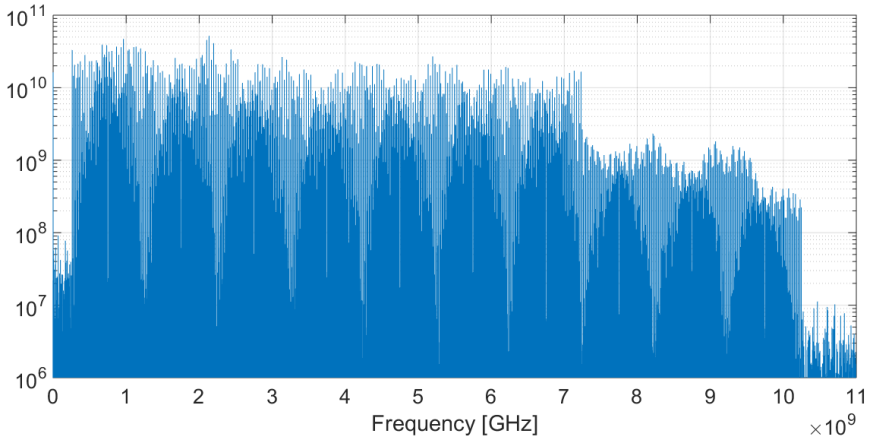

Figure 4.5: Received spectra: 34 Gb/s BTB.

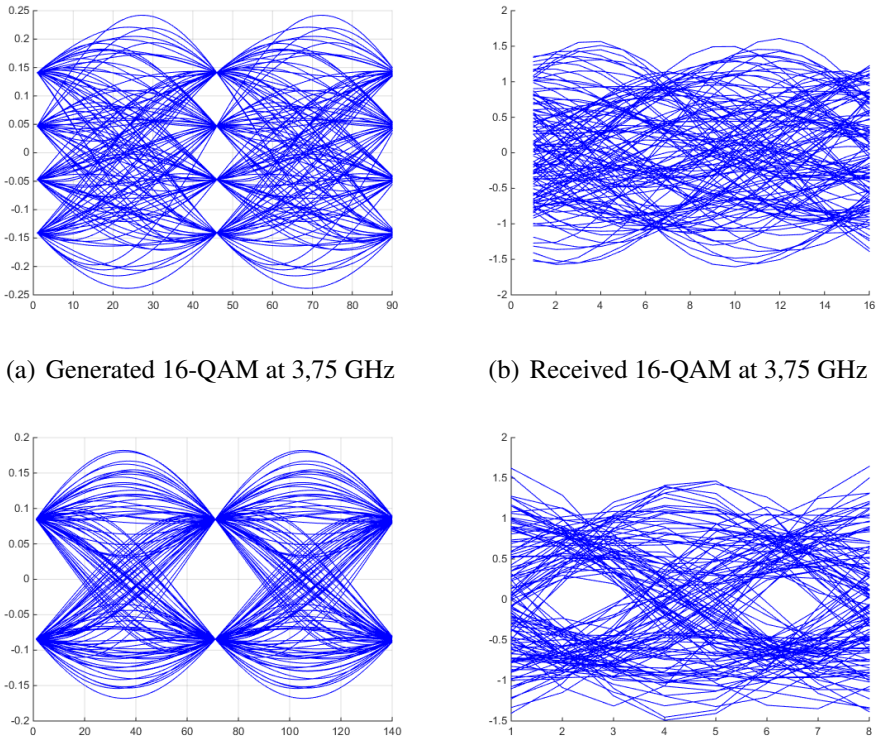

(a) Generated 16-QAM at 3,75 GHz

(b) Received 16-QAM at 3,75 GHz

(c) Generated 4-QAM at 8,75 GHz

(d) Received 4-QAM at 8,75 GHz

Figure 4.6: Eye diagrams related to the 34 Gb/s BTB transmission.

4.6(d) refer to respectively the generated and received eye diagram of the 4-QAM subcarrier at 8,75 GHz.

Despite the eye diagram related to the received 16-QAM at 3,75 GHz results quite closed, it is possible to recover the signal from the distortions induced by the chromatic dispersion and therefore guarantee the minimum fixed target BER, thanks to FFE/DFE equalization.

In Figure 4.7, the constellation diagrams of each subcarrier transmitted to reach 34 Gb/s in BTB are shown.

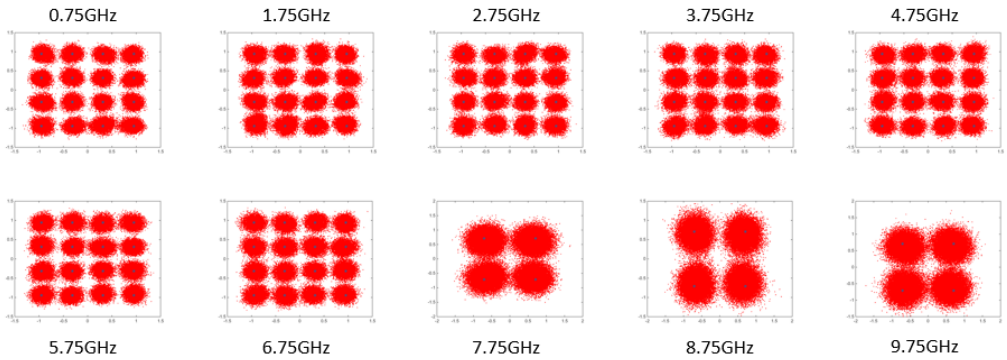

Figure 4.7: Constellation diagrams: 34 Gb/s BTB.

4.3 10 km SMF propagation performance

Over 10 km SMF propagation, the maximum transmission power results -7,4 dBm: the typical 0,2 dB/km fiber attenuation is verified (in BTB case the maximum transmission power is -5,4 dBm, see section 4.2). Unlike the BTB measurement case, propagation is now affected by chromatic dispersion (due to the fiber), which causes frequency fading (see Chapter 3, section 3.3.2). As shown in Figure 4.8, the system transfer function presents a deep frequency dip around 6 GHz. As a

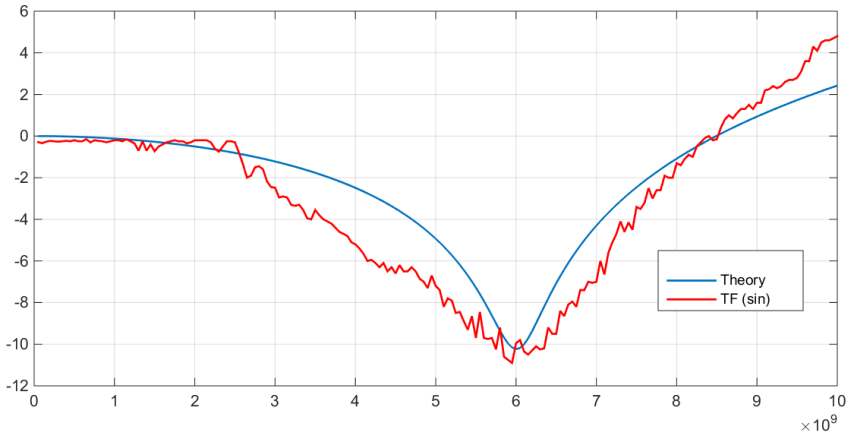

Figure 4.8: Frequency fading over 10 km SMF.

consequence, the subcarriers configuration employed in the BTB measurement case is no more possible. There are now different allocation costraints which require another modulation order of the subcarriers: higher data rate is assigned to the most

energy-efficient subcarriers, and lower data rate to the least energy-efficient ones (bit and power loading). According to these principles, the modulation order is set to 16-QAM (4 Gb/s bit rate), below 5,75 GHz, whereas to the frequencies affected by the dip, 5 GHz and 6 GHz, it is allocated a binary-PSK (BPSK) modulation (bit rate: 1 Gb/s). Above 6 GHz, 4-QAM (2 Gb/s bit rate) is employed, since the latest portion of the spectrum is attenuated (the spectral content of each component of the system limits the spectrum).

The details of the FDM modulation designed to maximize the system capacity over 10 km SMF are shown in Figure 4.9, with the relative BER of each subcarrier. Record bit rate of up 28 Gb/s is achieved, with -7,4 dBm transmission power.

16QAM @ 0.75 GHz bit rate: 4Gbps	16QAM @ 1.75 GHz bit rate: 4Gbps	16QAM @ 2.75 GHz bit rate: 4Gbps	16QAM @ 3.75 GHz bit rate: 4Gbps	16QAM @ 4.75 GHz bit rate: 4Gbps	BPSK @ 5.75 GHz bit rate: 1Gbps	BPSK @ 6.75 GHz bit rate: 1Gbps	4QAM @ 7.75 GHz bit rate: 2Gbps	4QAM @ 8.75 GHz bit rate: 2Gbps	4QAM @ 9.75 GHz bit rate: 2Gbps
BER_eq: 3.3E-03	BER_eq: 1.8E-03	BER_eq: 1.7E-03	BER_eq: 1.8E-03	BER_eq: 4E-04	BER_eq: 9.3E-04	BER_eq: 1.03E-04	BER_eq: 1.7E-03	BER_eq: 1.9E-03	BER_eq: E-03

Figure 4.9: 28 Gb/s over 10 km SMF.

The generated and received spectra related to the 28 Gb/s over 10 km SMF transmission are shown in Figure 4.10 and in Figure 4.11 respectively.

Figure 4.12(a) and Figure 4.12(b) show respectively an example of generated and received eye diagram (related to the 28 Gb/s transmission over 10 km SMF), in case of 16-QAM modulation of the subcarrier at 3,75 GHz; Figure 4.12(c) and Figure 4.12(d) refer to respectively the generated and received eye diagram of the 4-QAM subcarrier at 8,75 GHz; Figure 4.12(e) and Figure 4.12(f) refer to respectively the generated and received eye diagram of the BPSK subcarrier at 5,75 GHz.

In Figure 4.13, the sub-bands constellation diagrams of the 28 Gb/s over 10 km SMF transmission are shown.

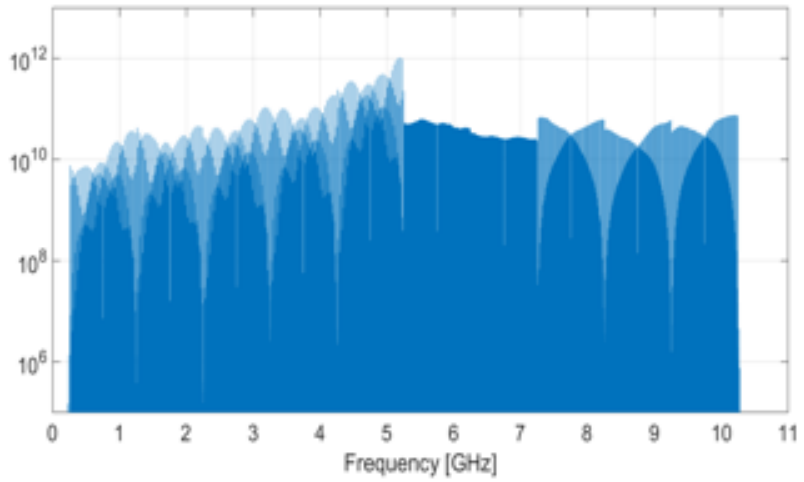

Figure 4.10: Generated spectra: 28 Gb/s over 10 km SMF.

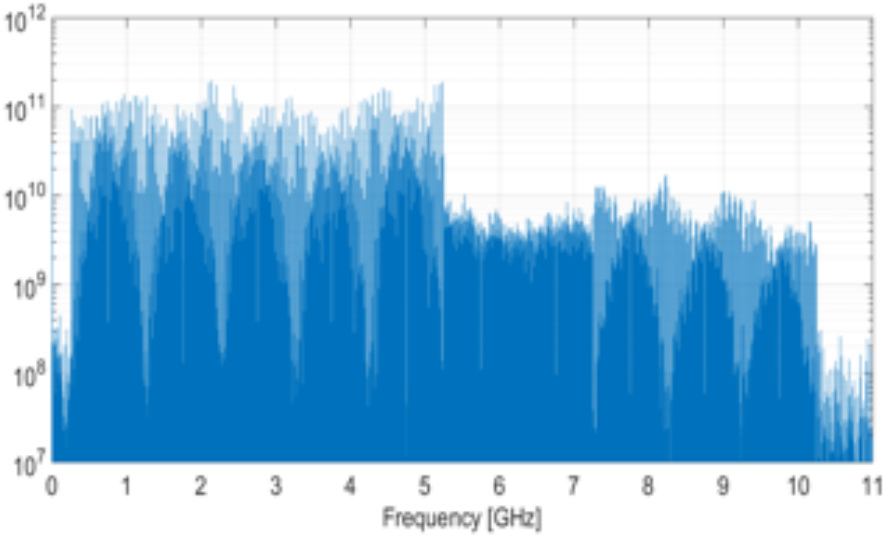

Figure 4.11: Received spectra: 28 Gb/s over 10 km SMF.

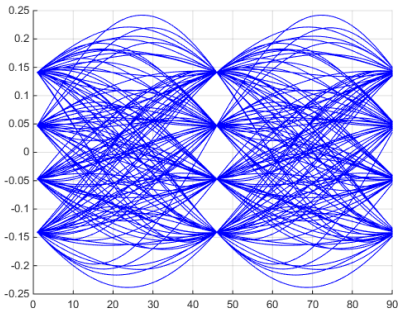

(a) Generated 16-QAM at 3,75 GHz

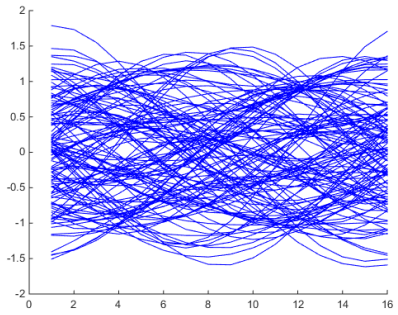

(b) Received 16-QAM at 3,75 GHz

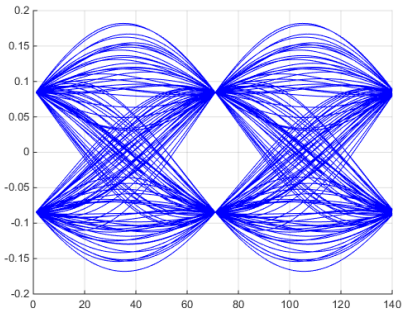

(c) Generated 4-QAM at 8,75 GHz

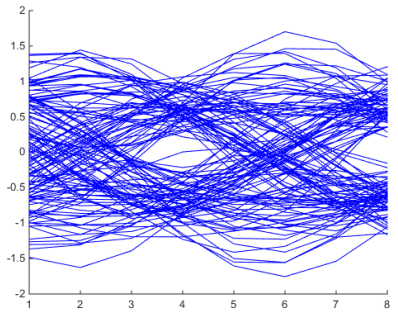

(d) Received 4-QAM at 8,75 GHz

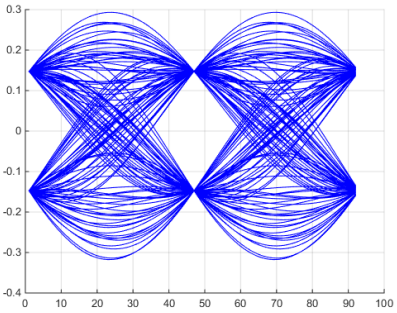

(e) Generated BPSK at 5,75 GHz

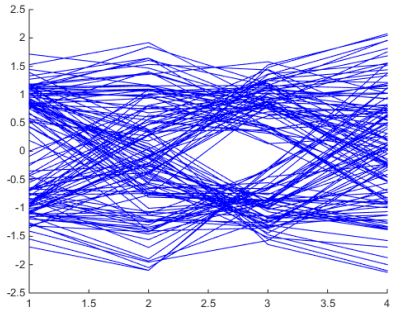

(f) Received BPSK at 5,75 GHz

Figure 4.12: Eye diagrams related to the 28 Gb/s transmission over 10 km SMF.

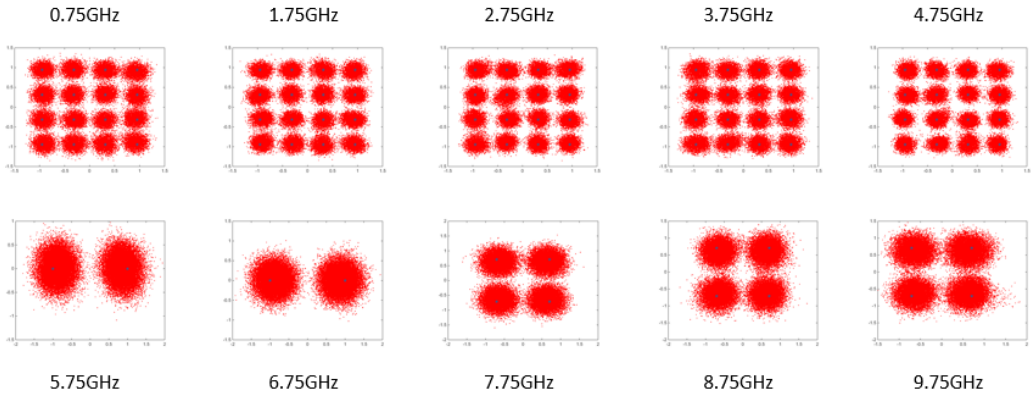

Figure 4.13: Constellation diagrams: 28 Gb/s over 10 km SMF.

Comparison with BTB In order to evaluate the transmission performance over 10 km SMF, the same configuration adopted to reach 28 Gb/s over 10 km SMF is transmitted in the BTB case. Figure 4.14 sums up the subcarriers transmission and their relative BER in this case, with -7 dBm transmission power.

16QAM @ 0.75 GHz bit rate: 4Gbps	16QAM @ 1.75 GHz bit rate: 4Gbps	16QAM @ 2.75 GHz bit rate: 4Gbps	16QAM @ 3.75 GHz bit rate: 4Gbps	16QAM @ 4.75 GHz bit rate: 4Gbps	BPSK @ 5.75 GHz bit rate: 1Gbps	BPSK @ 6.75 GHz bit rate: 1Gbps	4QAM @ 7.75 GHz bit rate: 2Gbps	4QAM @ 8.75 GHz bit rate: 2Gbps	4QAM @ 9.75 GHz bit rate: 2Gbps
BER_eq: 1.7E-04	BER_eq: 2E-04	BER_eq: 2.23E-04	BER_eq: 1.13E-04	BER_eq: 1.4E-04	BER_eq: 7E-04	BER_eq: 6.4E-04	BER_eq: 1.23E-04	BER_eq: 1.85E-04	BER_eq: 1.13E-04

Figure 4.14: 28 Gb/s BTB.

Figure 4.15 and Figure 4.16 show respectively the generated and received spectra in case of 28 Gb/s BTB transmission.

Figure 4.17(a) and Figure 4.17(b) show respectively the generated and received eye diagram (related to the 28 Gb/s BTB transmission), in case of 16-QAM modulation of the sub-band at 3,75 GHz; Figure 4.17(c) and Figure 4.17(d) show respectively the generated and received eye diagram of the 4-QAM subcarrier at 8,75 GHz; Figure 4.17(e) and Figure 4.17(f) refer to respectively the generated and received eye diagram of the BPSK sub-band at 5,75 GHz.

The constellation diagrams of each sub-band of the 28 Gb/s BTB transmission are shown in Figure 4.18.

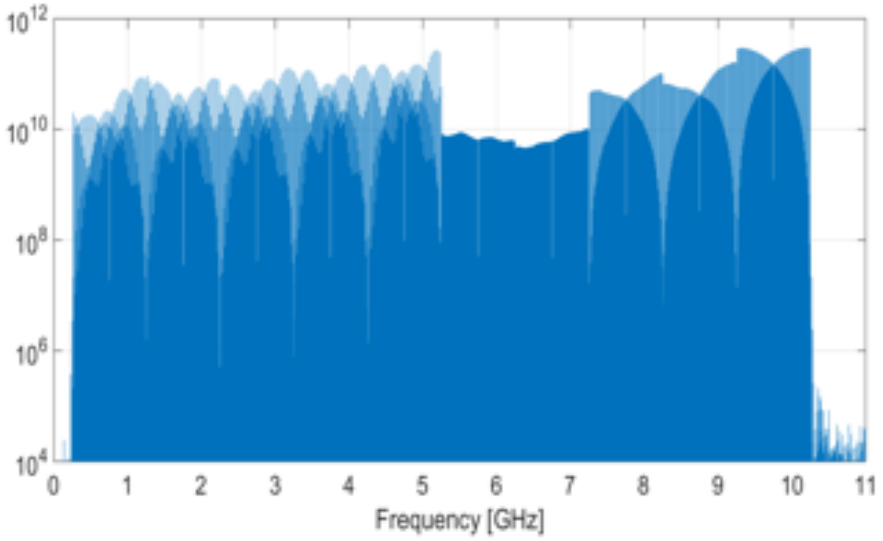

Figure 4.15: Generated spectra: 28 Gb/s BTB.

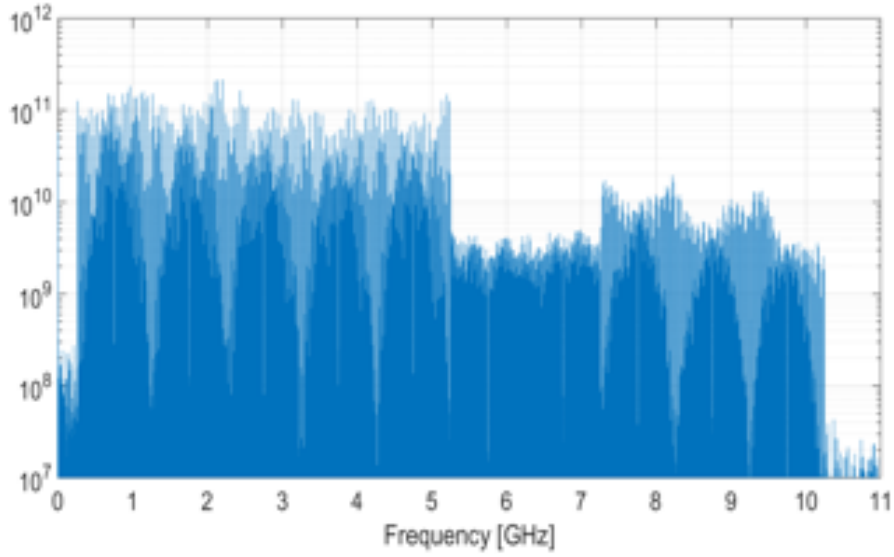

Figure 4.16: Received spectra: 28 Gb/s BTB.

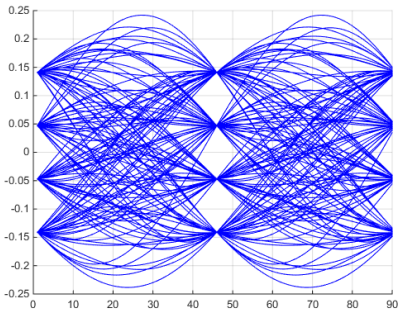

(a) Generated 16-QAM at 3,75 GHz

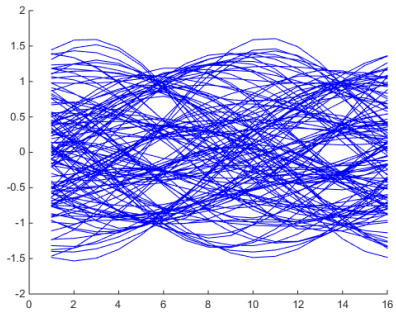

(b) Received 16-QAM at 3,75 GHz

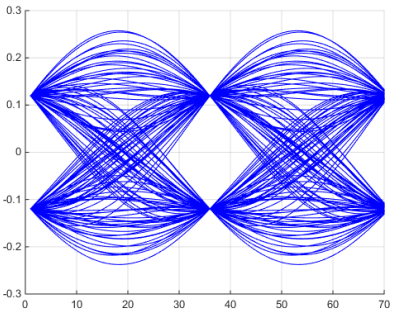

(c) Generated 4-QAM at 8,75 GHz

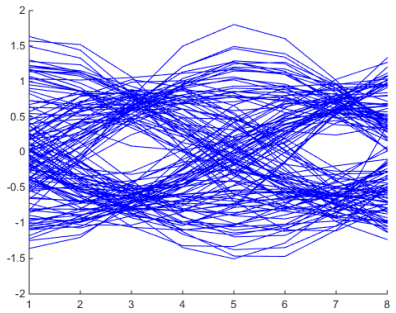

(d) Received 4-QAM at 8,75 GHz

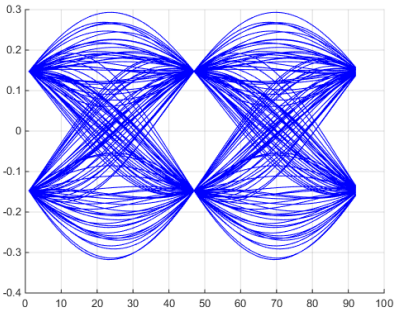

(e) Generated BPSK at 5,75 GHz

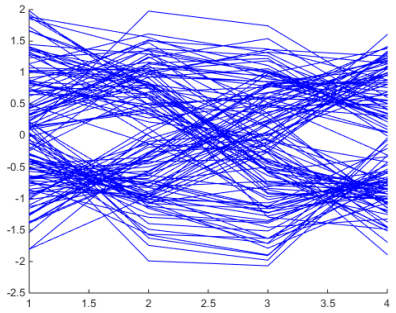

(f) Received BPSK at 5,75 GHz

Figure 4.17: Eye diagrams related to the 28 Gb/s BTB transmission.

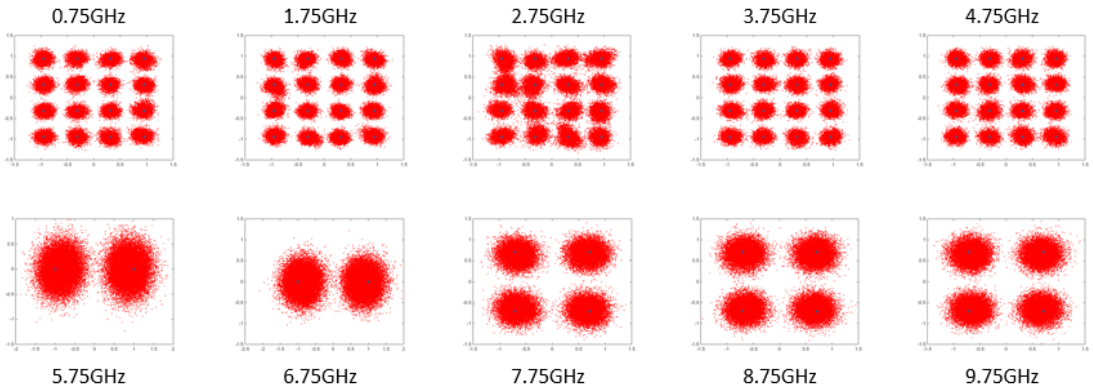

Figure 4.18: Constellation diagrams: 28 Gb/s BTB.

Figure 4.19 and Figure 4.20 show the BER curves for each subcarrier as the power changes, in case of BTB and 10 km SMF transmission respectively. It results a power penalty of about 3 dB, considering a target BER of 3×10^{-3} and a power of -7 dBm, in case of transmission over 10 km SMF with respect to the BTB case, although no significant degradation due to chromatic dispersion seems to be evident in the constellation diagrams.

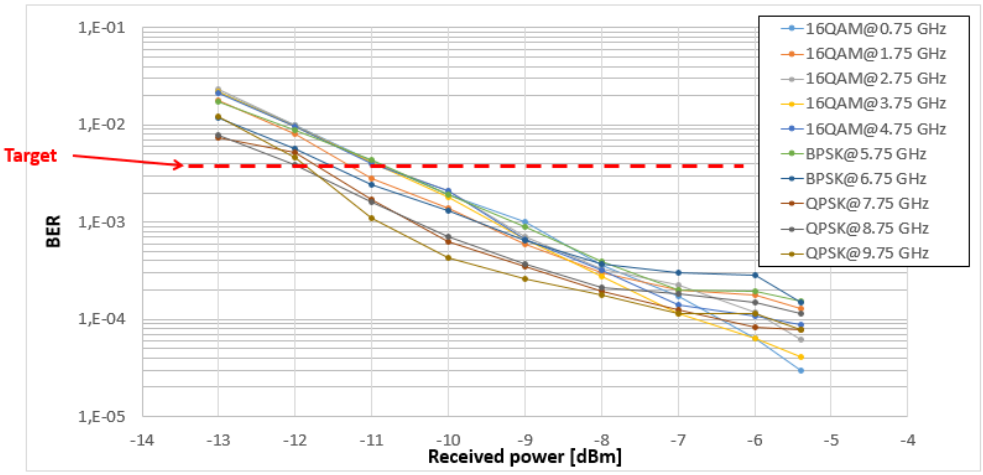

Figure 4.19: BER curves: 28 Gb/s BTB.

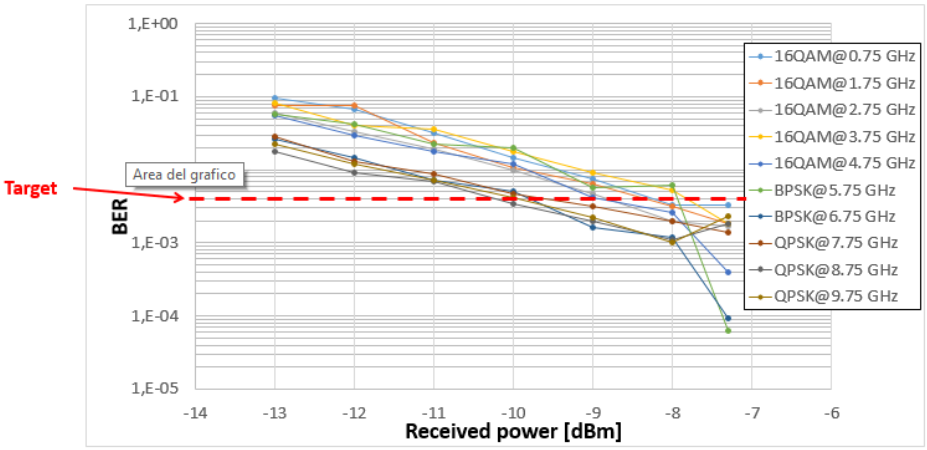

Figure 4.20: BER curves: 28 Gb/s over 10 km SMF.

4.4 20 km SMF propagation performance

Over 20 km SMF additional power constraints with respect to the BTB and 10 km SMF measurement cases affect the transmission: the maximum transmission power results -11,4 dBm. In order to provide the highest possible transmission power, the VOA is removed from the setup in Figure 4.1: the new maximum transmission power is -9,7 dBm (about 2 dBm power reduction with respect to the 10 km SMF measurement case).

As far as concerning the frequency fading caused by chromatic dispersion, a deep frequency dip is shown around 4 GHz in Figure 4.21. With respect to the 10 km SMF case, affected by fading around 6 GHz (see Figure 4.8), the frequency dip results shifted; another transmission configuration is therefore necessary. The least energy-efficient sub-band is now around 4,75 GHz, where a BPSK modulation (1 Gb/s bit rate) is employed, whereas the most energy-efficient ones are centered around 0,75 GHz, 1,75 GHz and 9,75 GHz. This last portion of the spectrum shows in fact a higher magnification of the frequencies with respect to the BTB and 10 km SMF cases (see Figure 4.2 and Figure 4.8 respectively), so that a 16-QAM allocation (bit rate: 4 Gb/s) results possible. The remaining sub-bands are set to 4-QAM modulation order (2 Gb/s bit rate). The details relative to this configuration are shown in Figure 4.22, where it is shown also the BER of each subcarrier. Total bit rate of up 25 Gb/s is achieved, with -9,7 dBm transmission power.

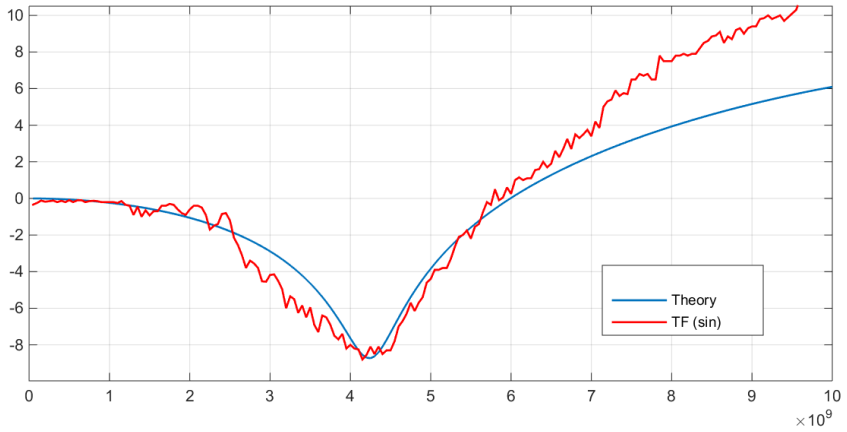

Figure 4.21: Frequency fading over 20 km SMF.

16QAM @ 0.75 GHz bit rate: 4Gbps	16QAM @ 1.75 GHz bit rate: 4Gbps	4QAM @ 2.75 GHz bit rate: 2Gbps	4QAM @ 3.75 GHz bit rate: 2Gbps	BPSK @ 4.75 GHz bit rate: 1Gbps	4QAM @ 5.75 GHz bit rate: 2Gbps	4QAM @ 6.75 GHz bit rate: 2Gbps	4QAM @ 7.75 GHz bit rate: 2Gbps	4QAM @ 8.75 GHz bit rate: 2Gbps	16QAM @ 9.75 GHz bit rate: 4Gbps
BER_eq: 1E-03	BER_eq: 1.1E-03	BER_eq: 2.7E-03	BER_eq: 1.2E-03	BER_eq: 6E-04	BER_eq: 1.9E-03	BER_eq: 1.3E-03	BER_eq: 1.3E-03	BER_eq: 1.3E-03	BER_eq: 1.5E-03

Figure 4.22: 25 Gb/s over 20 km SMF.

Figure 4.23 and Figure 4.24 show respectively the generated and received spectra related to the 25 Gb/s transmission over 20 km SMF.

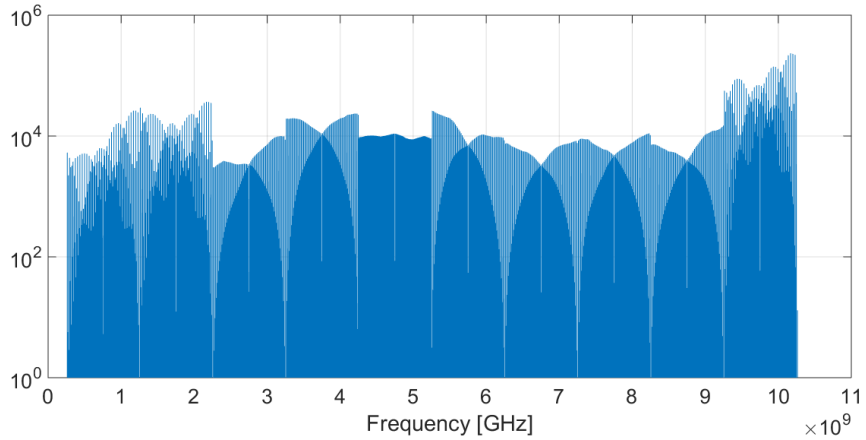

Figure 4.23: Generated spectra: 25 Gb/s over 20 km SMF.

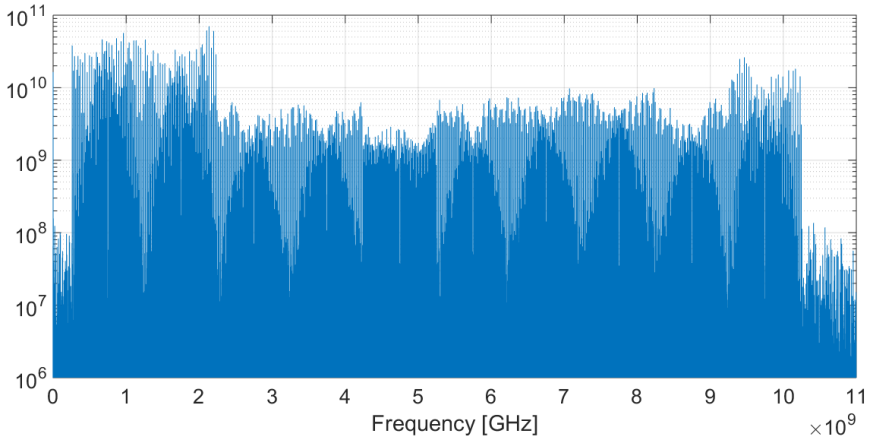

Figure 4.24: Received spectra: 25 Gb/s over 20 km SMF.

As far as concerning the eye diagrams, Figure 4.25(a) and Figure 4.25(b) show respectively the generated and received eye diagram (related to the 25 Gb/s transmission over 20 km SMF), in case of the 16-QAM subcarrier modulation at 9,75 GHz; Figure 4.25(c) and Figure 4.25(d) refer to respectively the generated and received eye diagram of the 4-QAM subcarrier at 8,75 GHz; Figure 4.25(e) and Figure 4.25(f) show respectively the generated and received eye diagram of the BPSK sub-band at 4,75 GHz.

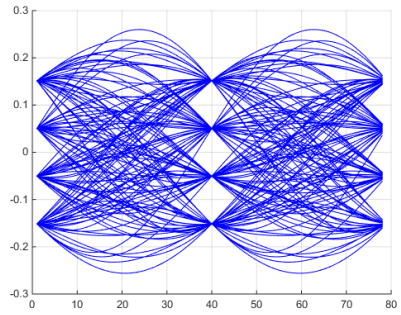

(a) Generated 16-QAM at 9,75 GHz

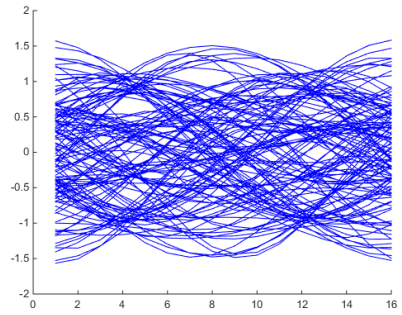

(b) Received 16-QAM at 9,75 GHz

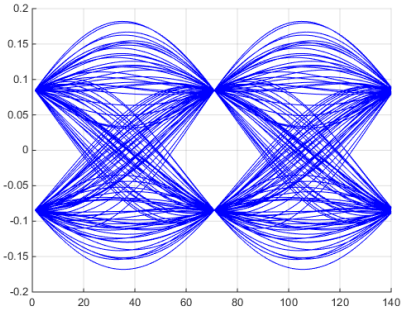

(c) Generated 4-QAM at 8,75 GHz

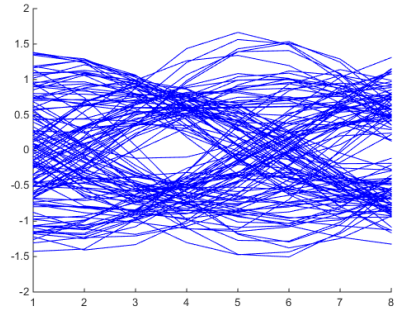

(d) Received 4-QAM at 8,75 GHz

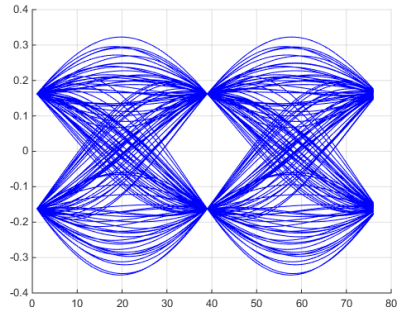

(e) Generated BPSK at 4,75 GHz

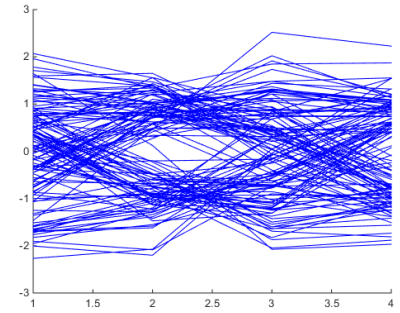

(f) Received BPSK at 4,75 GHz

Figure 4.25: Eye diagrams related to the 25 Gb/s transmission over 20 km SMF.

In Figure 4.26, the constellation diagrams relative to each sub-band of the 25 Gb/s transmission over 20 km SMF are shown.

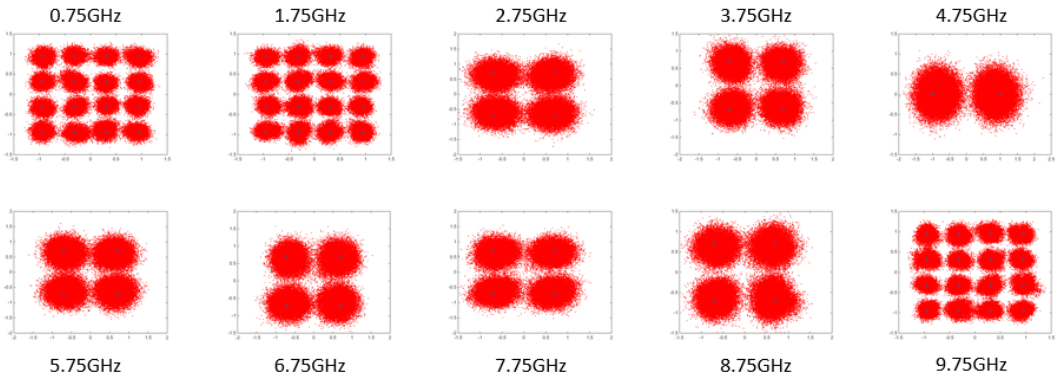

Figure 4.26: Constellation diagrams: 25 Gb/s over 20 km SMF.

4.5 On-off-keying as reference

In order to further understand the advantages in terms of capacity offered by FDM multicarrier transmission as regards the more efficient usage of the spectrum with respect to the single-carrier modulations, an experimental transmission of a binary baseband OOK signal over 10 km SMF is handled.

The system setup is the same as the previous FDM experiments (see Figure 4.1), as well as the working parameters: the I_{bias} is set to 9,5 mA, and the AWG peak to peak voltage, V_{pp}, to 300 mV.

With respect to the 28 Gb/s over 10 km SMF achieved by means of FDM modulation (see section 4.3), the reachable rate in case of baseband OOK transmission within the fixed 3.8×10^{-3} target BER, is limited to 12,5 Gb/s, with a maximum transmission power of -14 dBm, and BER $= 1,4 \times 10^{-3}$ (with FFE/DFE equalization). Figure 4.27(a) and Figure 4.27(b) show respectively the generated and received eye diagram of such baseband OOK signal over 10 km SMF, with 12,5 Gb/s capacity.

Despite the received eye diagram results quite closed, the FFE/DFE equalization allows to recover the signal from the distortions (mainly due to chromatic dispersion), and to guarantee the minimum fixed target BER.

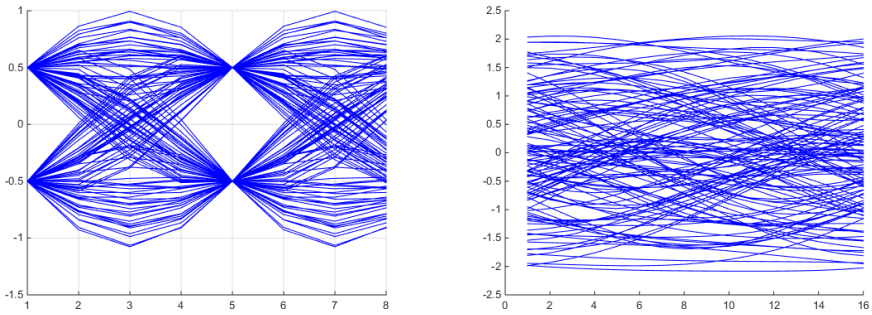

(a) Generated baseband OOK (b) Received baseband OOK

Figure 4.27: Eye diagrams related to the 12,5 Gb/s baseband OOK transmission over 10 km SMF.

4.6 Performance analysis

In the relatively short-range optical system scenario, where SMF is employed in order to reach distances up to few tens of kilometers, by means of long-wavelength VCSELs, the results discussed so far represent the achievement of an important transmission goal.

The state of the art results (see Chapter 1, section 1.8), are limited to 12,5 Gb/s with DMT modulation over 20 km SMF [7], whereas in this thesis 25 Gb/s are reached over 20 km SMF by using FDM. Moreover, the 28 Gb/s transmission here achieved over 10 km SMF represent record bit-rate of propagation along kilometer-SMFs. Also the BTB capacity of 34 Gb/s is an important result since it suggests a reachable capacity beyond 30 Gb/s in case of short-range applications of the order of few tens of meters, such as the data-center application.

In addition, it is significant to underline that the results obtained in this thesis are prominent considering the broad modulation bandwidth of the low-cost VCSEL employed: about 5-6 GHz. In literature it is common to employ even about 20 GHz modulation bandwidth, except for example the experimentation reported in [7], which exploits just 2,5 GHz bandwidth VCSEL.

Figure 4.28 sums up the achieved capacities as a function of the propagation distance.

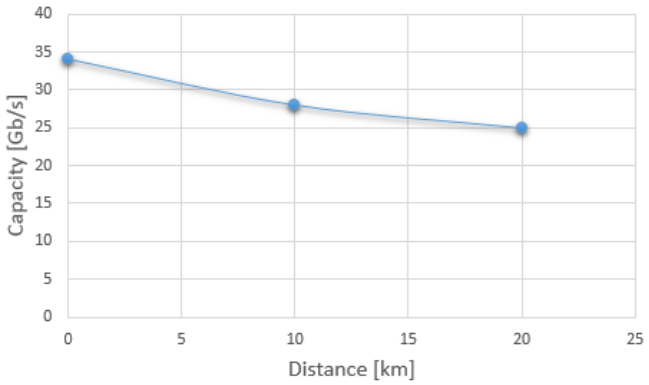

Figure 4.28: Capacitiy vs Distance Curve.

The results achieved in this thesis have been also subject to improvement attempts, but without any positive outcome.

In order to better distribute the power among the most energy-efficient sub-bands, a configuration without any subcarrier transmitted in correspondence of the dip has been tested. Such configuration consists of removing the two BPSK modulations at 5,75 GHz and 6,75 GHz from the one used to achieve 28 Gb/s over 10 km SMF, see section 4.3, Figure 4.9. The resulting BERs of the remaining subcarriers, however, do not suggest a substantial improvement with respect to the previous configuration, considering also that less information is transmitted.

Another attempt is handled as concerning the number of the subcarriers: the goal is to find a configuration with the same performances as those achieved by using the configuration related to the 28 Gb/s over 10 km SMF, but with less number of subcarriers. Following this target, at first the two BPSK modulations at 5,75 GHz and 6,75 GHz (see section 4.3, Figure 4.9) have been joined in a single BPSK modulation at 6,25 GHz. Then, the two 4-QAM sub-bands of the same configuration at 7,75 GHz and 8,75 GHz have been joined in a single 4-QAM sub-band at 8,25 GHz. In both cases, it results a loss of one order of magnitude as regards the joined sub-bands BERs with respect to the original configuration: narrower the subcarriers, more effective is the dispersion management. However, a further reduction of the subbarriers bandwidth occupancy, with respect to the 1 GHz allocated, would mean higher PAPR.

Therefore, it results not possible to further limit the number of the sub-bands while still remaining within the fixed $3,8 \times 10^{-3}$ target BER, or otherwise improve the performance.

Conclusions

Short-range data communication systems for consumer applications at the lower levels of the network represent a constant demand for more and more information throughput. It is the case of the metro and local-loop traffic applications, where low costs, robustness, easy handling, flexibility and scalability are required.

Optical solutions allow to reply to such increasing demand with simple technologies based on directly modulated VCSELs combined to IM/DD technique.

Simplicity and low costs features of such short-range systems come at the expense, however, of lower performance and lower spectral efficiency than long-haul systems.

In order to increase the reachable transmission bit-rate of this short-range scenario, different modulation formats have been exploited; they can be divided into single-carrier modulations and multicarrier transmissions.

Although single-carrier modulations, such as 4-PAM, show low complexity, high spectral efficiency and dispersion tolerance (through bit and power loading) can be achieved only with multicarrier transmissions, such as FDM, OFDM and DMT.

OFDM and DMT are however characterized by high PAPR and costly digital signal processing.

This thesis proposes therefore FDM in combination with multilevel modulation formats as transmission technique for short-range optical systems based on directly modulated long-wavelength VCSELs, with SMFs as transmission medium.

With respect to MMFs, in fact, SMFs let to achieve higher distances (up to few tens of kilometers), since they are not limited by the multimode dispersion.

Propagation is however affected by chromatic dispersion, which, combined to the frequency chirp induced by the VCSEL direct modulation, introduces frequency fading. Therefore, the number and the modulation order of the subcarriers in order to maximize the FDM transmission performance are investigated.

High performance transmission systems require also dispersion compensation techniques at the receiver side, thus FFE/DFE equalization is employed.

The goal of the work is to reach the highest possible capacity transmission in a short-range scenario. Following this purpose, the propagation is managed over different fiber lengths (10 km and 20 km SMF), as well as in the BTB case (which approximates the few meters order distances).

An AWG is used to directly modulate a 1580-nm VCSEL, while the FDM signal generation and post-processing is implemented via Matlab. For exploiting advanced FEC with 7% overhead, thus improving the quality of the transmission, a target BER of $3,8 \times 10^{-3}$ is fixed.

System parameters optimization, such as the use of a Nyquist pulse shaping with roll-off 0, electronic pre-equalization and frequency guard band, the warranty of working within the VCSEL linearity condition, and the choice of a proper amplitude for each sub-band depending on the system total TF, let to achieve important capacity results.

With the system components employed, in particular with the low-cost and narrow modulation bandwidth VCSEL used, and within the same target distances of 10 km and 20 km, as well as within the fixed $3,8 \times 10^{-3}$ target BER, it is demonstrated that the achieved results can not be further improved.

With respect to the 12,5 Gb/s achieved in case of baseband OOK transmission over 10 km SMF, the FDM technique allows to reach a capacity of 28 Gb/s on the same system: it is a record transmission rate considering also the results obtained in literature over kilometer-SMFs. State of the art results are limited to 12,5 Gb/s with DMT over 20 km SMF, while in this thesis FDM permits 25 Gb/s along the same SMF distance.

The shortest range applications can be exemplified in this thesis by the BTB measurement case, in which 34 Gb/s transmission is achieved with FDM.

The obtained performances are particularly significant considering the broad modulation bandwidth of the employed VCSEL (5-6 GHz). Therefore, in order to further improve the results, future works could be managed employing a higher performance VCSEL, with for example 20 GHz modulation bandwidth, like the ones proposed and employed also in literature.

Bibliography

[1] K. Szczerba, P. Westbergh, J. Gustavsson, A. Haglund, J. Karout, M. Karlsson, P. Andrekson, E. Agrell, and A. Larsson, "Towards 40gbps downstream fdm pon," *ECOC Technical Digest*, 2011 OSA.

[2] S. Lee, *Discrete Multitone Modulation for Short-Range Optical Communications*, T. U. Eindhoven, Ed., 2009.

[3] A. Lebreton and B. Charbonnier, "Towards 40gbps downstream fdm pon," *Optical Network Design and Modeling (ONDM)*, 2013, 17th International Conference.

[4] W. Peng, X. Wu, V. Arbab, K. Feng, B. Shamee, L. Christen, J. Yang, A. Willner, and S. Chi, "Theoretical and experimental investigations of direct-detected rf-tone-assisted optical ofdm systems," *JOURNAL OF LIGHTWAVE TECHNOLOGY, VOL. 27, NO. 10*, May 2009.

[5] W. Shieh and I. Djordjevic, *OFDM for optical communications*, E. A. Press, Ed., 2010.

[6] M. Martinelli, *Optical Communications*, lecture notes.

[7] T. N. Duong, N. Genay, P. Chanclou, B. Charbonnier, J. L. Masson, and M. Ouzzif, "Maximizing the transmission performance of dmt signal for next generation pon system by direct modulation of cost-effective and low bandwidth lasers," *OSA/OFC/NFOEC*, 2009.

[8] T. Pham, R. Rodes, J. B. Jensen, C. J. ChangHasnain, and I. T. Monroy, "Sub-cycle qam modulation for vcsel-based optical fiber links," *OSA*, 2013.

[9] F. Karinou, R. Rodes, K. Prince, I. Roudas, and I. T. Monroy, "Im/dd vs. 4-pam using a 1550-nm vcsel over short-range smf/mmf links for optical interconnects," *OFC/NFOEC Technical Digest*, 2013 OSA.

[10] R. Rodes, M. Müeller, B. Li, J. Estaran, J. B. Jensen, T. Gruendl, M. Ortsiefer, C. Neumeyr, J. Rosskopf, K. J. Larsen, M. Amann, and I. T. Monroy, "High-speed 1550 nm vcsel data transmission link employing 25 gbd 4-pam modulation and hard decision forward error correction," *JOURNAL OF LIGHTWAVE TECHNOLOGY,VOL.31,NO.4*, FEBRUARY 2013.

[11] K. Szczerba, P. Westbergh, M. Karlsson, P. Andrekson, and A. Larsson, "60 gbits error-free 4-pam operation with 850 nm vcsel," *ELECTRONICS LETTERS, Vol. 49, No. 15*, July 2013.

[12] K. Szczerba, P. Westbergh, J. Gustavsson, A. Haglund, J. Karout, M. Karlsson, P. Andrekson, E. Agrell, and A. Larsson, "30 gbps 4-pam transmission over 200m of mmf using an 850 nm vcsel," *ECOC Technical Digest*, 2011 OSA.

[13] A. Larsson, J. S. Gustavsson, A. Haglund, J. Bengtsson, B. Kögel, P. Westbergh, R. Safaisini, E. Haglund, K. Szczerba, M. Karlsson, and P. Andrekson, "High speed vcsels for optical interconnects," *IPRM International Conference*, August 2012.

[14] S. Lee, F. Breyer, S. Randel, D. Cárdenas, H. van den Boom, and A. Koonen, "Discrete multitone modulation for high-speed data transmission over multimode fibers using 850-nm vcsel," *OSA/OFC/NFOEC*, 2009.

[15] K. Szczerba, B. Olsson, P. Westbergh, A. Rhodin, J. S. Gustavsson, A. Haglund, M. Karlsson, A. Larsson, and P. A. Andrekson, "37 gbps transmission over 200 m of mmf using single cycle subcarrier modulation and a vcsel with 20 ghz modulation bandwidth," *Proceedings of 36th European Conference on Optical Communication, paper We.7.B.2.*, 2010.

[16] "Il mondo delle telecomunicazioni," http://www.ilmondodelletelecomunicazioni.it/.

[17] K. Szczerba, P. Westbergh, J. Karout, J. Gustavsson, A. Haglund, M. Karlsson, P. Andrekson, E. Agrell, and A. Larsson, "4-pam for high-speed short-range

optical communications," *JOURNAL OPTICAL COMMUNICATION NETWORKS, VOL. 4, NO. 11*, NOVEMBER 2012.

[18] K. Szczerba, P. Westbergh, E. Agrell, M. Karlsson, P. A. Andrekson, and A. Larsson, "Comparison of intersymbol interference power penalties for ook and 4-pam in short-range optical links," *JOURNAL OF LIGHTWAVE TECHNOLOGY, VOL. 31, NO. 22*, NOVEMBER 2013.

[19] "Wiley encyclopedia of telecommunications," http://onlinelibrary.wiley.com/.

[20] L. Reggiani, *Wireless Communications*, lecture notes.

[21] L. Nadal, M. S. Moreolo, J. F'abrega, A. Dochhan, H. Grießer, M. Eiselt, and J. Elbers, "Dmt modulation with adaptive loading for high bit rate transmission over directly detected optical channels," *JOURNAL OF LIGHTWAVE TECHNOLOGY, VOL. 32, NO. 21*, NOVEMBER 2014.

[22] S. Lee, F. Breyer, S. Randel, D. Cárdenas, H. van den Boom, and A. Koonen, "Discrete multitone modulation for high-speed data transmission over multimode fibers using 850-nm vcsel," *OSA/OFC/NFOEC*, 2009.

[23] Y. Gao, J. Yu, J. Xiao, Z. Cao, F. Li, and L. Chen, "Direct-detection optical ofdm transmission system with pre-emphasis technique," *JOURNAL OF LIGHTWAVE TECHNOLOGY,VOL.29,NO.14*, JULY 2011.

[24] "Radio-electronics.com," http://www.radio-electronics.com/.

[25] "Ert," http://www.electronics-radio.com/.

[26] B. Schmidt, A. Lowery, and J. Armstrong, "Experimental demonstrations of electronic dispersion compensation for long-haul transmission using direct-detection optical ofdm," *JOURNAL OF LIGHTWAVE TECHNOLOGY, VOL. 26, NO. 1*, JANUARY 2008.

[27] "Rp photonics encyclopedia," http://www.rp-photonics.com/.

[28] P. KREHLIK, "Characterization of semiconductor laser frequency chirp based on signal distortion in dispersive optical fiber," *OPTO-ELECTRONICS REVIEW 14(2), 123–128*, 2006.

[29] D. Derickson, *Fiber Optic Test and Measurement*, P. Hall, Ed., 1997.

[30] M. Bobula, A. Prokeš, and K. Daněk, "Nyquist filters with alternative balance between time- and frequency-domain parameters," *EURASIP Journal on Advances in Signal Processing*, 2010.

[31] E. Iannone, *Telecommunication Networks*, C. Press, Ed., 2011.

[32] "Use forward error correction to improve data communications," http://www.electronicdesign.com/.

[33] I.-T. R. G.975.1, Ed., *Forward error correction for high bit-rate DWDM submarine systems*.

[34] "Soft-decision fec benefits for 100g," http://www.fujitsu.com/.

[35] "Eblana photonics," http://www.eblanaphotonics.com/.

[36] Tektronix, Ed., *Understanding AWG70000A Series Frequency Response and DAC Performance, application note*.

[37] L. A. Neto, D. Erasme, N. Genay, P. Chanclou, Q. Deniel, F. Traore, T. Anfray, R. Hmadou, and C. Aupetit-Berthelemot, "Simple estimation of fiber dispersion and laser chirp parameters using the downhill simplex fitting algorithm," *JOURNAL OF LIGHTWAVE TECHNOLOGY,VOL.31,NO.2*, 2012.

[38] J. Wang and K. Petermann, "Small signal analysis for dispersive optical fiber communication svstems," *JOURNAL OF LIGHTWAVE TECHNOLOGY,VOL.10,NO.1*, January 1992.

[39] A. Rnyset, L. Bjerkan, D. Myhre, and L. Hafskjzr, "Use of dispersive optical fibre for characterisation of chirp in semiconductor lasers," *ELECTRONICS LETTERS, Vol. 30, No. 9*, April 1994.